Marine and Petroleum Geology 170 (2024) 107131

Contents lists available at ScienceDirect

Marine and Petroleum Geology

journal homepage: www.elsevier.com/locate/marpetgeo

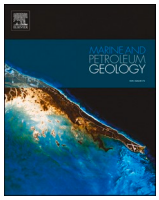

Chemostratigraphy and mineralogical characterization of Piacenzian sapropels cluster A (2.75–2.57 Ma) in the Gelasian GSSP type-section of Monte San Nicola (Sicily, Italy): Paleoenvironmental and paleogeographic implications

Stefano Fasone [a], Giovanna Scopelliti [a,*], François Baudin [b], Antonio Caruso [c]

[a] Dipartimento di Scienze della Terra e del Mare, Università di Palermo, Palermo, Italy
[b] Institut des Sciences de la Terre de Paris, Sorbonne Université, CNRS, Paris, France
[c] Dipartimento di Scienze e Tecnologie Biologiche, Chimiche e Farmaceutiche, Università di Palermo, Palermo, Italy

ARTICLE INFO

Keywords:
Lower pleistocene GSSP
Sapropel cluster A
TOC
Mineralogy
Geochemistry
Paleoceanographic model

ABSTRACT

Mineralogical, geochemical and stable isotope ($\delta^{18}O$, $\delta^{13}C$) data from Marine Isotope Stages (MIS) G4 to 103 are here presented. The studied interval includes the sapropelic cluster A (A2-A5) from the Gelasian GSSP type-section, outcropping at Monte San Nicola (Sicily, Italy). The studied section exhibits a good response of the $\delta^{18}O$ measured on the bulk carbonate to the Earth's astronomical parameters. The sapropelic red/brown layers (A2- A5) are alternated to grey marls and this cyclicity is clearly evident by the difference in colour, organic matter content, redox-sensitive elements and runoff indicators, tied to the precession/insolation cycles. Further, the obliquity signal is well evident in paleoproductivity indicators and mineralogical composition, driven by glacial-interglacial cycles. The obtained dataset has allowed the reconstruction of the paleoenvironmental conditions during marls/sapropels deposition, which appears to be influenced by the precessional forcing that induced strong changes in the marine water circulation. This scenario is also integrated by an original paleogeographic model including the presence of a high topographic structure in SE Sicily that limited water exchanges between the Ionian and Central Mediterranean Seas during sea level drawdowns, caused by glacial phases, triggered by obliquity minima.

1. Introduction

The Gelasian GSSP was proposed at the Monte San Nicola type-section ($MSN_{t\text{-}s}$) by Rio et al. (1998), between the villages of Gela and Butera (Sicily, Italy). It was placed at the top of the sapropel "Nicola bed", equivalent to the A5 sapropel (Hilgen, 1991a) and corresponds to the insolation cycle i-250 within Marine Isotopic Stage (MIS) 103. As firstly described by Channell et al. (1992), the Gelasian GSSP almost coincides with the Gauss/Matuyama reversal and it was defined as the third stage of the Pliocene (Rio et al., 1994). The importance of the Monte San Nicola GSSP was further emphasized in 2010 when the base of the Pleistocene/Quaternary was shifted from the top of the Gelasian to its base (Gibbard and Head, 2010; Gibbard et al., 2010). Thus, the Gelasian GSSP represents the boundary between Pliocene-Pleistocene Series and Neogene-Quaternary Systems.

From a global climatic perspective, the Gelasian GSSP falls within a period of continental reorganization due to the progressive closure of the Panama Isthmus (Haug and Tiedemann, 1998; Haug et al., 2001; Schmidt, 2007) that influenced the global oceanic and atmospheric circulation. In particular, the Panama Isthmus starting the uplift during the Miocene (i.e. Schmidt, 2007) with a progressive closure developed in several steps during the Pliocene, completing its closure between 3 and 2.5 Ma (Haug and Tiedemann, 1998; O'Dea et al., 2016). The presence of the Isthmus strengthened the North Atlantic thermohaline circulation, bringing moisture to the Arctic polar region, allowing the formation of North Atlantic Deep Water and establishing the Arctic ice caps with glacial-interglacial cycles (Bartoli et al., 2005).

In particular, from 2.75 to 2.57 Ma the obliquity-driven glacial periods intensified, with a significant expansion of the Arctic ice caps but only from MIS 100 the sea level significantly dropped, becoming similar

* Corresponding author.
E-mail address: giovanna.scopelliti@unipa.it (G. Scopelliti).

https://doi.org/10.1016/j.marpetgeo.2024.107131
Received 10 July 2024; Received in revised form 19 September 2024; Accepted 23 September 2024
Available online 26 September 2024

to that recorded during the Pleistocene glaciations, even if with different estimations (Jakob et al., 2020; Miller et al., 2020). This interval is characterized by cyclic alternation of sapropels/marls as described in the eastern Mediterranean Sea ODP boreholes (Kidd et al., 1978; Emeis et al., 1996; Grant et al., 2017, 2022) and in Mediterranean land outcrops (Hilgen, 1991a; Rio et al., 1994; Lourens et al., 1996; Castradori et al., 1998; Caruso, 2004; Cita et al., 2008; Beltran et al., 2021).

In the central Mediterranean Sea, the formation of sapropels started at 3.08 Ma (Hilgen, 1991a; Lourens et al., 1996; Caruso, 2004). It is linked to increasing temperature and rainfall due to monsoon activity in northern Africa and is precessionally controlled (Rossignol-Strick et al., 1982; Rossignol-Strick, 1983), as also evidenced by lower $\delta^{18}O$ values (Rohling, 1994; Rohling et al., 2015) and higher temperatures (Herbert et al., 2015). According to Hilgen (1991a), sapropel mid points coincide with precessional minima/insolation maxima, during which the difference in insolation, between summer and winter, was maximized, leading to an expansion of the Intertropical Convergence Zone (ITCZ) northward (Larrasoaña et al., 2013). During these warm-humid periods (precessional minima), the Mediterranean circulation underwent a drastic change, with the formation of warmer extensive surface freshwater in the uppermost part of the sea water column, characterized by negative excursions in the $\delta^{18}O$ values (Rossignol-Strick et al., 1982; Vergnaud-Grazzini, 1985), that prevented the formation of more oxygenated bottom water (Emeis et al., 2000, 2003). This configuration predisposed the eastern-central Mediterranean basin to the formation of deep hypoxic/anoxic environments, with the consequent better preservation of organic matter at the seabed, a process that led to the formation of sapropelic levels. Other authors (Schrader and Matherne, 1981; Thunell and Williams, 1982; Henrichs and Reeburgh, 1987) suggest that sea bottom anoxia resulted from increases productivity due to the influx of nutrients during Green Sahara periods, through rivers that discharged into the southern Mediterranean basin.

Until today, only four high-resolution studies have been conducted on the Gelasian GSSP type-section (Channell et al., 1992; Sprovieri, 1993; Radmacher et al., 2023; Addante et al., 2024), essentially focused on calcareous plankton assemblages and stable oxygen isotopes whilst other studies have been performed in the coeval interval at the "Mandorlo" section, outcropping 400 m west from the GSSP type section (Becker et al., 2005; Capraro et al., 2022; Zanola et al., 2024). Further, although less recently, Becker et al. (2005) performed a high-resolution study on $\delta^{18}O$ benthic foraminiferal record in the interval between MIS 101–99 underlining the usefulness of the $MSN_{t\text{-}s}$ for detailed paleoclimatic and paleoenvironmental studies.

Despite the high importance of the Gelasian GSSP, and its great

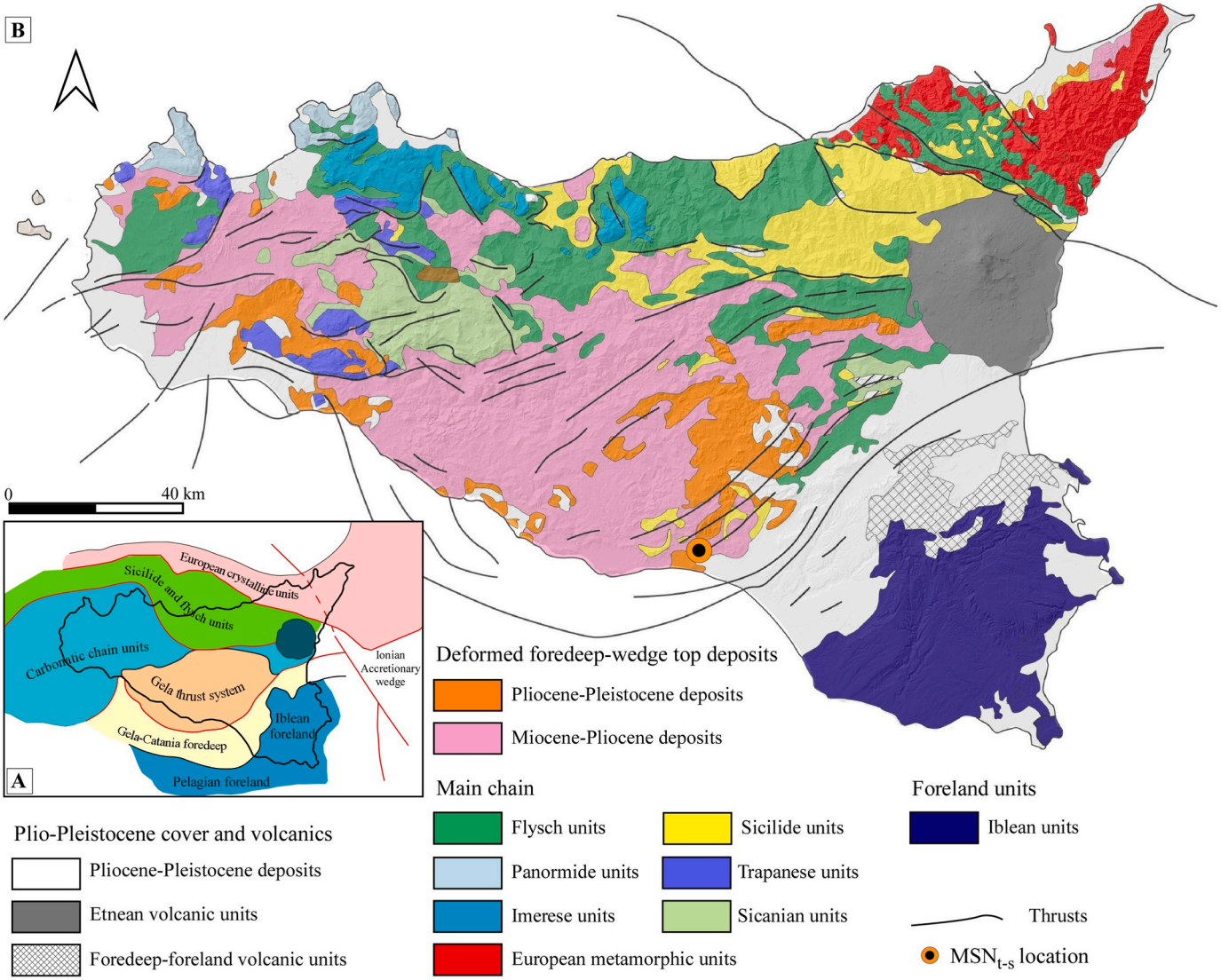

Fig. 1. A) Schematic structural framework of Sicily, modified from Gasparo Morticelli et al. (2015); B) Regional geological-structural map of Sicily modified from Lentini and Carbone (2014) and Gasparo Morticelli et al. (2015). $MSN_{t\text{-}s}$: Monte San Nicola type-section.

potential as reference section for the Lower Quaternary interval, no detailed geochemical-mineralogical studies have been performed in the type-section. The aim of this work is to characterize the paleoclimate and paleoenvironmental history of the Central-Southern Mediterranean during the deposition of the sapropel cluster A sensu Hilgen (1991a), between 2.75 and 2.58 Ma, corresponding to MIS G4-103. In particular, three are the main goals of this study: (i) to evaluate the effects of the orbital forcing on the oxygen and carbon isotopes measured on the bulk carbonate, also evaluating the possible effect of diagenesis on the $MSN_{t\text{-}p}$; (ii) to reconstruct the depositional conditions in terms of variations in surface productivity, continental inputs, redox conditions at the seafloor and organic carbon preservation; (iii) to provide new insights into the paleoceanographic context of this sector of the Mediterranean Sea by the proposal of an original palaeogeographic model.

2. Geological and stratigraphic context

The $MSN_{t\text{-}s}$ crops out in central-southern Sicily, between the villages of Gela and Butera and it is located in the Caltanissetta Basin, a Neogene structure positioned between the front of the Sicilian-Maghrebian Apennine chain and the Hyblean foreland (Catalano et al., 2013) (Fig. 1A). During the Plio-Pleistocene this structure represented a foredeep basin, overlying the Gela Nappe (Ogniben, 1969), an allochthonous unit thrust above the deformed units of the Cretaceous/Paleogene (Amerillo Fm.) and the Numidian Flysch (Lentini and Carbone, 2014; Gasparo Morticelli et al., 2015) (Fig. 1B). Presently, the relief of Monte San Nicola is encompassed within the Gela Thrust system, characterized by deep Pleistocene active thrusts during the late Gelasian and early Calabrian. Along the southern slope of MSN, the sedimentary succession is well exposed with a continuous sequence from Lower Pliocene to Lower Pleistocene (Fig. 2A). The Trubi Fm., Zanclean/Piacenzian in age, is here 36 m thick and it is constituted by the classical quadruplet, precessionally controlled, made by whitish calcareous marls alternated to grey/beige marly limestones (Hilgen, 1991a). Sediments of Trubi Fm. Are rich in calcareous microfossils (coccolithophorids and foraminifera), deposited in a bathyal environment between 700 and 1000 m depth (Sgarrella et al., 1997). Upwards the sequence continues with 125 m of grey/brownish marls alternated to reddish/black clays and marly clays (sapropels), belonging to the Monte Narbone Fm. (Hilgen, 1991b) (Fig. 2B). These sediments were deposited at the bathymetry comprising 200–700 m depth, during the late Piacenzian and Calabrian (Caruso, 2004; Sprovieri et al., 2006). The badlands of the southern slope of the Monte Narbone Fm. host four sapropelic clusters (O, A, B, and C) already described by Hilgen (1991a) (Fig. 2). This formation includes the entire Gelasian Stage and its GSSP, placed at the top of sapropel A5. Upwards the Monte Narbone Fm. becomes richer in silt and sand and the topmost part of the outcrop is characterized by 15 m of yellowish calcarenites belonging to the Agrigento Fm. (Calabrian), rich in molluscs and sedimented in outer and inner shelf environments, between 20 and 200 m. Some particular layers are crossed laminated, deposited in very shallow water at bathymetries less than 30 m. The whole section lies on discordance, with a tectonic thrust, over the Numidian Flysch. This latter unit is constituted of brownish silty-clays and siltstones lower Miocene in age.

3. Materials and methods

3.1. Sampling and age model

The studied interval is the same published by Addante et al. (2024). It is represented by a ~9 m thick continuous and undisturbed section belonging to the Monte Narbone Fm. (Fig. 2). The sampled interval mainly consists of massive whitish marls (average thickness of ~135 cm) alternating with grey marly clays and darker clays (average thickness of ~31 cm), here considered as sapropels A2 to A5. In this study, 44 samples already studied by Addante et al. (2024) were selected, with a sampling resolution ranging from 5 to 50 cm.

The A5 sapropel represents the last layer of cluster A related to i-cycle 250, called Nicola bed (Nb). The Gelasian GSSP, placed at the top of Nb, is 17.5 cm above the sapropel mid-point, astronomically dated at 2.588 Ma by Lourens et al. (1996), as also reported by Capraro et al. (2022). Thus, according to Lourens et al. (2004) the Pleistocene started

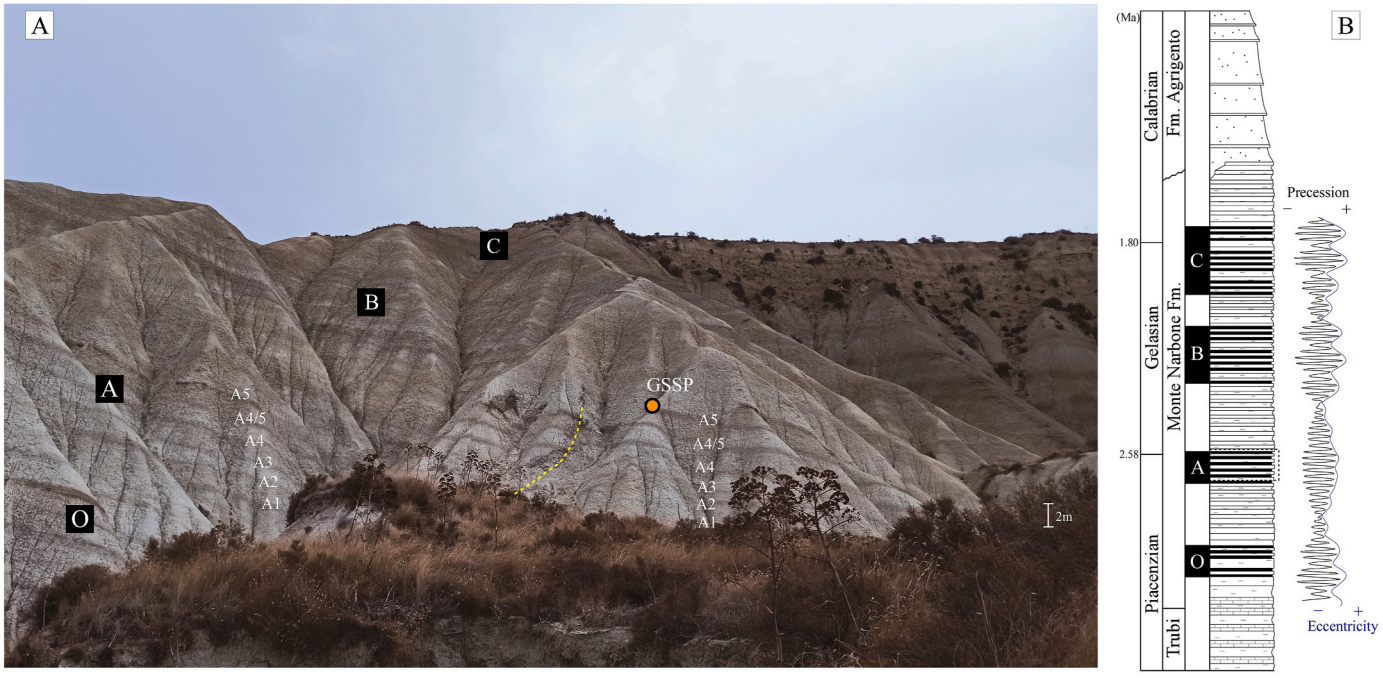

Fig. 2. A) Field view of the Monte San Nicola badlands hosting the Gelasian GSSP (orange circle); dotted yellow line: sampling section; B) Chrono- and lithostratigraphy of the Monte San Nicola section showing the sapropelitic clusters O, A, B, and C (also reported in A) and their correlation with the precession and eccentricity curves from Laskar et al. (2004).

at ~2.58 Ma. Recently, Addante et al. (2024) did not consider a 3-kyr time lag for the astronomical tuning of the sapropels, thus the Nb mid-point was dated at 2.905 Ma. In this work the age model proposed by Addante et al. (2024) was adopted, thus the studied section spans the interval from 2.694 to 2.582 Ma and all the data presented below are reported with respect to the age.

3.2. Colour analysis

Colour analysis was conducted on the pressed, powdered samples under a standardized artificial light source at 6000 K. Due to minimal chromatic variation, a digital approach through image acquisition under controlled parameters was preferred to the use of standard Munsell charts.

The colour of each sample was determined through digital analysis of the data, utilizing a high-resolution photo (4000 × 3000 pixels). The RGB (Red, Green, and Blue) value of each sample was then defined on a uniform area of 50 × 50 pixels. In addition, the obtained colour was converted to greyscale by averaging the intensity values of the RGB components. According to the RGB colour model, the greyscale value falls within the range of 0–255, where 0 (R = 0, G = 0, B = 0) corresponds to black and 255 corresponds to white, with intermediate values representing shades of grey, darker as they approach 0.

3.3. Mineralogical analysis

Bulk mineralogy was determined at the DiSTeM (University of Palermo) by powder X-ray diffraction (XRD) using a Philips PW141373 diffractometer with a Cu Kα radiation filtered by a monochromator crystal and a 3°2θ/minute scanning speed. Qualitative interpretation of the diffractograms were performed with the support of the HighScore Plus v3.0e software utilizing the Crystallography Open Database v2014 (COD_OCT 2014; Gražulis et al., 2009). Semi-quantitative estimation was carried out using the area method.

3.4. Stable oxygen and carbon isotopes

Carbon and oxygen stable isotope composition were determined on the bulk samples at the DiSTeM (University of Palermo) using a Thermo Scientific Delta V Advantage mass spectrometer. CO_2 was obtained by the classical H_3PO_4–$CaCO_3$ reaction method, at 50 °C, coupled to an automated carbonate preparation device (Thermo Scientific GasBench II). The isotopic compositions are expressed in δ‰ units relative to the international V-PDB standard, using the international standard NBS19 ($\delta^{18}O_{V\text{-}PDB} = -2.20‰$ and $\delta^{13}C_{V\text{-}PDB} = 1.95‰$) measured every 20 samples, and an internal reference standard (Carrara marble MAB, $\delta^{18}O_{V\text{-}PDB} = -2.43‰$ and $\delta^{13}C_{V\text{-}PDB} = 2.43‰$), analyzed every 10 samples. The latter was also used to calculate the measurement repeatability (σ), which was found to be < 0.1‰ for both carbon and oxygen.

3.5. Total organic carbon

A quantitative and qualitative study of the organic matter content was performed using a Rock–Eval 6 Turbo apparatus (Vinci Technologies) at the Institut des Sciences de la Terre de Paris (UMR7193/Sorbonne Université). The Total Organic Carbon (TOC) was obtained by means of Rock-Eval thermal analysis, on around 65 mg of powdered samples, following the method described by Lafargue et al. (1998) and Behar et al. (2001). TOC content is expressed as weight percentage (wt %), with precision of ±0.1%. The type of kerogen was estimated using the Hydrogen Index (HI, in mgHC/gTOC) standard parameter, whereas the thermal maturation of the organic matter was assessed using the T_{max} parameter expressed in °C (Baudin, 2024).

3.6. Geochemical elements

Geochemical analysis were performed at the ActLabsLtd (Ancaster, ON, Canada) measuring major, minor, and trace elements. After a 4 Acid "Near Total" Digestion, a part of the elements (Al, P, Ti, Co, Ni, Cu, Zn, and Pb) were determined by ICP/OES, the others (Mg, K, Ca, Mn, Fe, V, Cr, As, Rb, Zr, Ba, Th, and U) by ICP/MS. The preparation procedure (more details on https://actlabs.com/geochemistry/exploration-geochemistry/4-acid-near-total-digestion/) does not allow measuring Si directly using ICP, for this reason the concentrations of Si were obtained by difference to 100% subtracting all other major element concentrations and the LOI (measured at 1000 °C) (Liu et al., 2009).

Quality control of the analysis was conducted by measuring a blank every 40 samples, an internal control every 20 samples, and analyzing 8 certified standards. The precision was calculated based on duplicate analyses and expressed in terms of Relative Standard Deviation (RSD), with RSD <2% for Mg, Al, K, Ca, Mn, Fe, and for Co, Zn, Ba, Th, and U; RSD ranging between 2 and 5% for P, V, Ni, Cu, Rb, Zr, and Pb, and between 5 and 10% for Ti, Cr, and As.

4. Results

4.1. Lithological log and organic carbon characterization

The lithological log, as defined by Addante et al. (2024), has here been integrated with the calcium carbonate content determined by Rock-Eval analysis, together with the chromatic variation determined on the studied samples also converted into grayscale (Fig. 3). Further, the lithological log is integrated with TOC content whose characterization in terms of hydrogen indexes (HI) is summarized in Table 1. In the $MSN_{t\text{-}s}$, the colour well distinguishes the boundaries of light marly-clayey levels from darker and reddish-brown marly beds, here considered as sapropels. The sapropels are sometimes characterized by higher content of organic matter and variable lamination. In particular, TOC percentages oscillate between 0.16 and 0.4% with the highest value coinciding with the A5 sapropel (Nb). On the contrary, marly-clayey levels are characterized by organic carbon content between 0.08 and 0.12% with HI averagely higher in the marls levels with respect to the sapropels (132 against 109 mgHC/gTOC), while no variations in T_{max} with respect to the lithology are documented slightly fluctuating around a value of 392 °C (Table 1).

Following Hilgen (1991b), the term "sapropel" was adopted for all the darker and reddish-brown silty-marly beds belonging to sapropelic cluster A, even though the TOC content is lower than the sapropel threshold of 2% as defined by Kidd et al. (1978).

4.2. Mineralogy

The mineralogy of the analyzed samples is summarized in Table 1 and the profile along the section of the main phases are reported in Fig. 3. Calcite cyclically oscillates showing strong variations between marls and sapropels, being more abundant in the marls with values between 45 and 70%, and reaching minima values, between 20 and 40%, in the sapropels. Unlike calcite, quartz exhibits large cyclical variations (Fig. 3), increasing in the sapropels with an average value of 11%, up to 16% in the upper part of sapropel A5 (2.590 Ma), and lower concentrations in the marls (mean values of 8%). Similarly, clay minerals display large and well-defined oscillations between marls and sapropels, being more abundant in sapropels and less in marls (Fig. 3). Regarding the accessory mineral phases (Table 1), dolomite is markedly more abundant in the marls and is always present in sapropels except in the A5 sapropel while feldspars show the highest abundances in sapropels although the maximum value (17%) was recorded in a marly level between sapropels A4/5 and A5 (2.605 Ma).

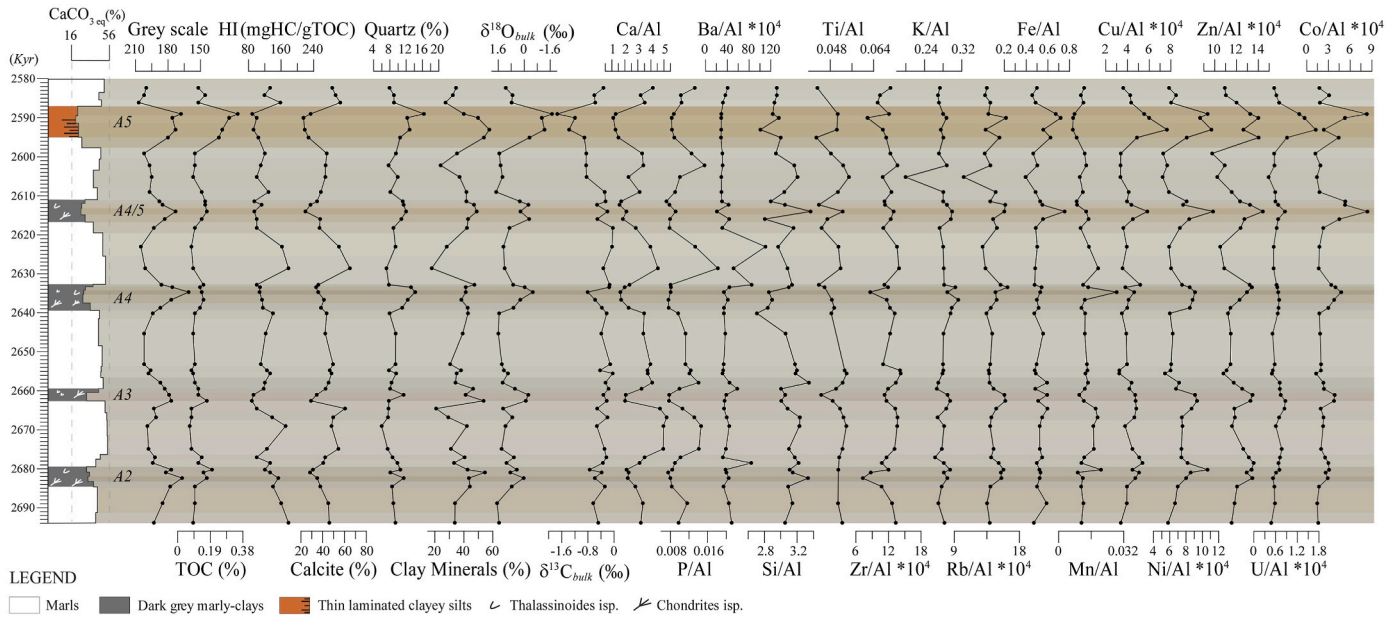

Fig. 3. Variations over time of the all proxies investigated in this study. Lithological log: modified by Addante et al. (2024) with the integration of the calcium carbonate equivalent percentage measured by Rock-Eval analysis; background: RGB colour of samples determined as described in section 3.2; A2 to A5: sapropels investigated in the $MSN_{t\text{-}s}$.

Table 1
Average value and variation range of the minerals abundance and geochemical proxies determined in marls and sapropels at the $MSN_{t\text{-}s}$.

	Sapropels			Marls		
	Mean	Min	Max	Mean	Min	Max
Grey scale	178	161	188	197	185	207
$CaCO_3$ eq (%)	30.64	19.91	44.57	46.61	38.82	53.65
TOC (%)	0.18	0.1	0.35	0.10	0.07	0.16
HI (mgHC/gTOC)	109	88	153	132	100	178
T_{max} (°C)	395	383	427	389	381	410
Calcite (%)	33	22	43	47	37	65
Quartz (%)	11	8	16	8	6	10
Clay Min. (%)	46	38	58	34	18	43
Dolomite (%)	3	0	5	5	2	9
Feldspar (%)	7	0	12	6	0	17
$\delta^{18}O_{bulk}$ (‰)	−0.05	−1.70	0.86	1.24	0.64	1.72
$\delta^{13}C_{bulk}$ (‰)	−0.57	−1.74	−0.14	−0.39	−0.86	−0.04
Si/Al	3.01	2.75	3.36	3.12	2.71	3.34
P/Al	0.008	0.007	0.010	0.012	0.008	0.018
K/Al	0.29	0.27	0.31	0.27	0.20	0.30
Ca/Al	1.96	1.11	3.28	3.76	2.28	5.21
Ti/Al	0.04	0.03	0.05	0.05	0.04	0.05
Mn/Al	0.012	0.007	0.028	0.014	0.010	0.019
Fe/Al	0.56	0.48	0.75	0.51	0.40	0.60
Co/Al *10^4	4.16	1.69	8.39	1.91	1.20	2.99
Ni/Al *10^4	8.83	6.76	11.31	6.54	5.11	8.67
Cu/Al *10^4	4.81	3.81	7.64	3.95	3.24	5.39
Zn/Al *10^4	13.05	11.44	14.42	11.52	9.76	13.57
Rb/Al *10^4	15.06	13.33	16.36	13.83	10.30	15.13
Zr/Al *10^4	11.01	7.27	12.96	12.78	10.78	14.25
Ba/Al *10^4	38.52	20.80	84.82	41.36	28.92	110.28
U/Al *10^4	0.81	0.53	1.71	0.60	0.41	0.84

4.3. Stable isotope geochemistry

In Fig. 3, bulk oxygen and carbon stable isotopes are plotted. The $\delta^{18}O_{bulk}$ values range from −1.70 to 1.72‰, with a mean value of −0.05‰ in sapropels and 1.29‰ in marls, respectively. Oxygen isotope fluctuations closely follow the alternations between sapropels and marls, exhibiting strong excursions towards lower values in sapropels. The trend is quite similar to $\delta^{18}O_{G.\ bulloides}$ even though this latter shows more marked oscillations above all into the marls.

The $\delta^{13}C_{bulk}$ values range from −1.74 to −0.04‰, with a mean of −0.57‰ in sapropels and −0.38‰ in marls. The carbon isotope fluctuations weakly follow the lithology in the interval A2–A4/5, with decreasing values in the sapropels and showing lower ratios in A4 and A5 sapropels, the latter characterizing by the lowest values (−1.74‰). In particular, $\delta^{13}C_{bulk}$ exhibits a clear decrease from A4/5 to A5.

4.4. Elemental geochemistry

The behaviour of major, minor, and trace elements was investigated by normalizing their concentrations to aluminum. The results are presented in Figs. 4 and 5. The normalization to a conservative element is a common practice that helps to mitigate the so-called “closed-sum effect” (Rollinson, 2014) and the choice of aluminum as conservative element is driven by its minimal disturbance from biological, diagenetic, and redox processes (Löwemark et al., 2011). For these reasons, it is particularly suitable for normalizing elements in sedimentary environments where fictitious oscillations may occur due to variations in carbonates and organic matter.

An overview of the mean values, together with the variation ranges, of the geochemical proxies is reported in Table 1.

4.4.1. Paleoproductivity proxies

Similarly to the calcite, the Ca/Al ratio (Fig. 4) closely follows the lithological signal, decreasing in sapropels and increasing in marls. It is worth to note that the values are higher in the marls between sapropels A2–A3 and A4–A4/5, reaching a median value of 4.4 and 3.8 respectively, while they are lower between sapropel A3–A4 and A4/5–A5, reaching a median value of 3.6 and 3. The maximum value of 5.2 is reached in the marls between A2 and A3, between 2.673 and 2.664 Ma, whereas the minimum value of 1.1 is reached in the mid-point of sapropel A5 (2.593–2.590 Ma).

Phosphorus is an essential element for the trophic chain and being included among the nutrient elements it is associated with the organic matter, mainly in phytoplankton remains (Tribovillard et al., 2006). P/Al shows a similar trend to Ca/Al ratio and follows the lithological signal with the highest values into marls and the lowest in the sapropels. The values are higher in the marl levels between sapropels A2–A3 and

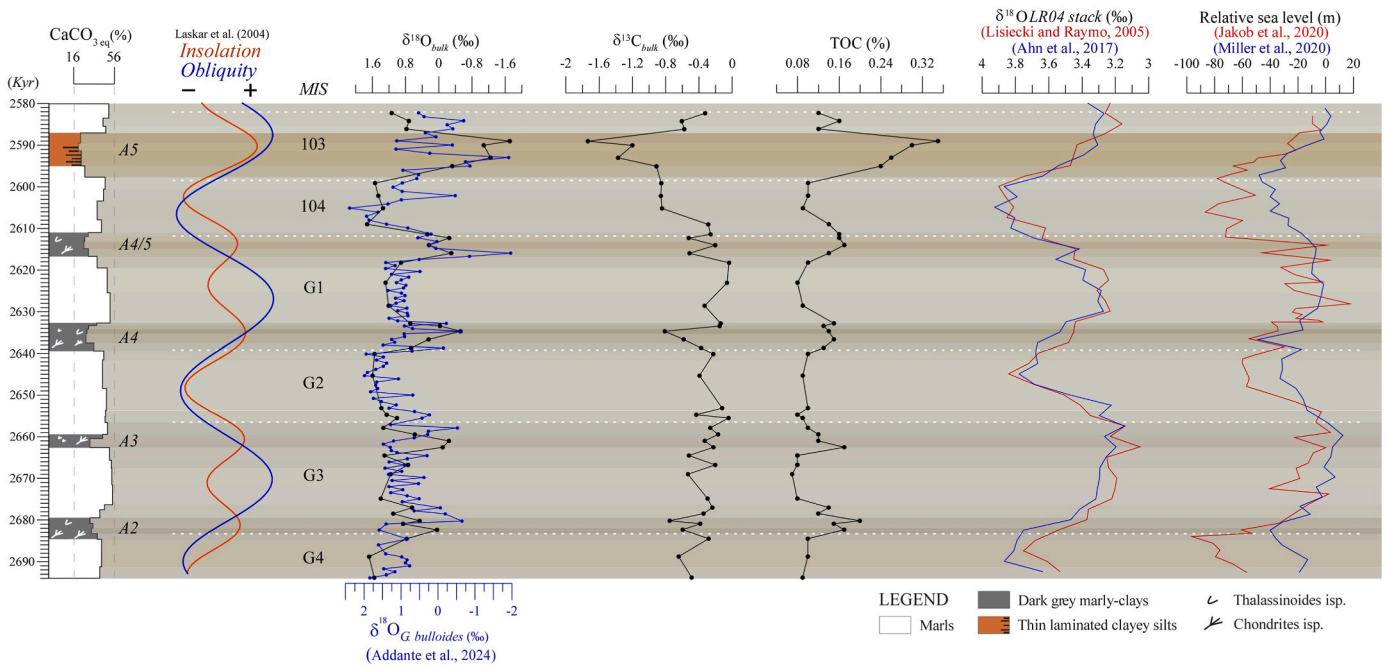

Fig. 4. Variations over time of the bulk oxygen and carbon stable isotope ratios and TOC (profiles in black) at the $MSN_{t\text{-}s}$. Figure also reports: the $\delta^{18}O$ measured on the *G. bulloides* from Addante et al. (2024) in the same samples (blue profile); the curves of obliquity (blue) and insolation at 65°N (red) from Laskar et al. (2004); the Marine Isotopic Stages (MIS G4 to 103); the $\delta^{18}O$ of the 'benthic stack LR04' from Lisiecki and Raymo (2005) and the 'Prob-LR04-stack' from Ahn et al. (2017); the relative sea level variations from Jakob et al. (2020) and Miller et al. (2020). Lithological log, colour background and A2 to A5 as in Fig. 3.

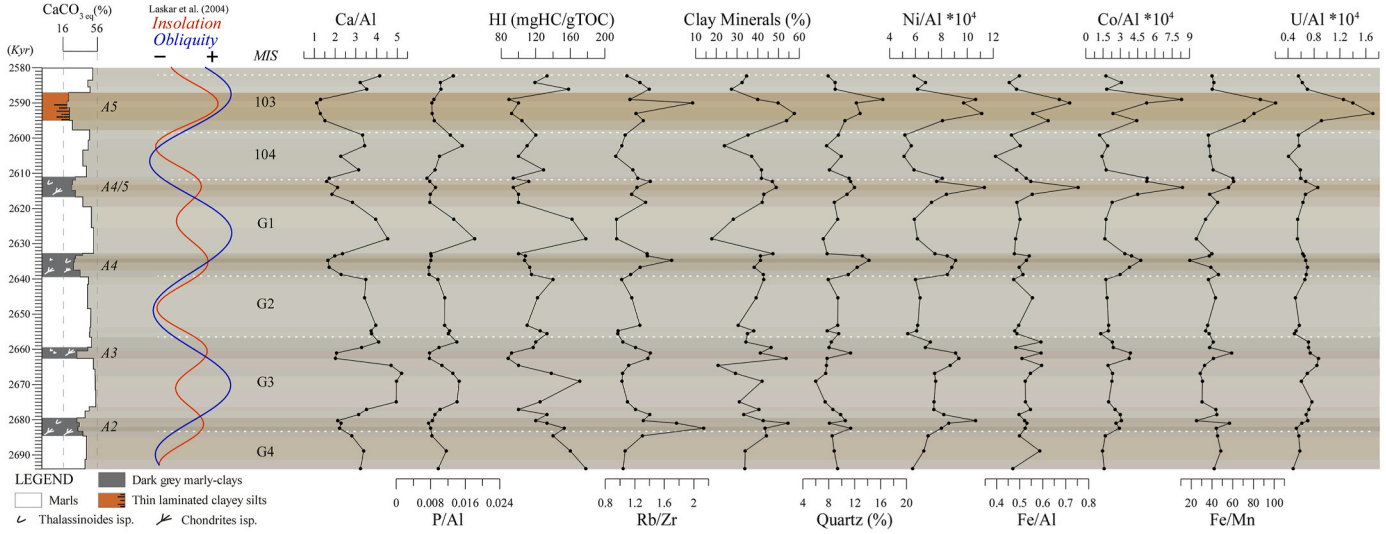

Fig. 5. Variations over time of the proxies discussed in section 5.2. Lithological log, colour background, A2 to A5 and astronomical curves as in Fig. 3.

A4–A4/5, reaching a median value of 0.013, while they are lower between sapropels A3–A4 and A4/5–A5, reaching a median value of 0.011. The maximum value of 0.018 is reached in the marly layer between sapropels A4/5–A5, while the minimum value of 0.0071 is reached within sapropel A4/5. Barium, like phosphorus, is a constituent of the organic matter being commonly associated with the biological activity (e.g. Dymond et al., 1992). Throughout the $MSN_{t\text{-}s}$, Ba/Al ratio is characterized by two sharp peaks, rispectivelly above the sapropels A2 and A3 and a wide increase in the marls between the sapropels A4 and A4/5 (up to 110) (Fig. 3).

4.4.2. *Continental input indicators*

Silicium in pelagic sediments can be mainly related to silicates (quartz, feldspars, clay minerals) from continental inputs and/or increased productivity associated with diatoms and radiolarians shells. Throughout the studied section, the Si/Al shows a general decreasing trend upward in the section not clearly correlated with the lithological variations (Fig. 3). Minimum value of 2.7 is reached in a marl just below the sapropel A4 and the maximum within the sapropel A4/5.

Titanium and zirconium are elements associated with inputs of Saharan eolian dust as they are contained in heavy minerals such as zircon, titanite, and rutile (Wehausen and Brumsack, 2000; Scheuvens et al., 2013; Martinez-Ruiz et al., 2015). In the $MSN_{t\text{-}s}$, variations in the Ti/Al and Zr/Al ratios (Fig. 3) follow the lithological variations, decreasing in the sapropels and increasing in the marls. Ti/Al reach minimum values of 0.028, 0.030 and 0.029 within the sapropels A2, A4 and A5, respectively. The same levels are characterized by the minimum values of Zr/Al 7.2, 8.6 and 8.4 ($*10^{-4}$), respectively.

On the contrary, potassium and rubidium are elements associated with continental runoff as they are contained in illite and feldspars (Wehausen and Brumsack, 2000; Martinez-Ruiz et al., 2015). Throughout the studied succession, variations in the K/Al and Rb/Al ratios are related to the lithology with higher values in the sapropels (Fig. 3). Both ratios reach the maximum value in the sapropel A4 (0.31 for K/Al and $16.35*10^{-4}$ for Rb/Al), and are characterized by a sharp decrease to values of 0.19 (for K/Al) and $10.3*10^{-4}$ (for Rb/Al) in the marls between the sapropels A4/5 and A5.

4.4.3. Redox-sensitive elements

The major element involved in the redox reactions are iron and manganese due to their ability to assume different oxidation numbers. In the $MSN_{t\text{-}s}$, the Fe/Al profile shown in Fig. 3 exhibits a significant increase in the ratio in the sapropels A4/5 and A5, reaching values of 0.75 and 0.71. The increases are modest in the sapropels A3 and A4 and essentially negligible in A2. The Mn/Al ratio (Fig. 3) is moderately higher in the marls between sapropels A2–A3 and A4–A4/5 (average value of 0.016 and 0.015, respectively), while it is lower in the remaining marly levels (mean value of 0.014; Table 1). Two sharp peaks are recorded inside the sapropel A4 and at the top of the sapropel A2 (0.028 and 0.021, respectively).

As for the trace elements, the Ni/Al, Cu/Al, and Zn/Al ratios show a similar trend (Fig. 3) increasing in sapropels with respect to the marly levels. The Cu/Al ratio reach the maximum value of 7.63 inside the sapropel A5. The Ni/Al and Zn/Al instead reach their maximum value, of 11.3 and 14.4 respectively, inside the sapropel A4/5.

Other elements sensitive to redox conditions but associated with the terrigenous fraction are uranium and cobalt. The depth profile of the U/Al ratio (Fig. 3) increase in the sapropels with the exception of the sapropel A2. In particular, the sapropel A5 is characterized by a U/Al ratio (1.7) more than double of the value recorded in the other sapropelic levels. The sapropels are best marked by the Co/Al ratio (Fig. 3) with maximum values in the sapropels A4/5 and A5 (8.39 and 8.30, respectively).

5. Discussion

5.1. Bulk isotope stratigraphy and orbital forcing

In order to evaluate the possible influence of a diagenetic component that may have altered the original signal, the $\delta^{18}O_{bulk}$ have been compared with the $\delta^{18}O_{G.\ bulloides}$ recently published by Addante et al. (2024) (Fig. 4).

The two profiles are well correlated and the bulk isotopic signal has better adherence to grey intensity compared to $\delta^{18}O_{G.\ bulloides}$ reported by Addante et al. (2024). The perfect overlap of the isotopic ratios obtained on the two different matrices demonstrates the absence of carbonate cement precipitation, which in the case of burial diagenesis or late interaction with meteoric waters would have resulted in a shift of the $\delta^{18}O$ towards lighter values in the bulk sample (i.e. Dickson and Coleman, 1990). Irrelevant thermal diagenesis is also testified by low T_{max} values, on average, <395 °C and always lower than 427 °C (Table 1).

The similarity in values also suggests that the isotopic signal recorded by the bulk samples is predominantly representative of the photic zone. This is in agreement with Beltran et al. (2007) who, studying the interval between 3.01 and 2.91 Ma at the Punta Piccola section (Piacenzian GSSP, Sicily), found that the $\delta^{18}O_{bulk}$ was predominantly composed of calcareous nannofossils and planktonic foraminifera, with small differences between marls and sapropels. This also supports the use of calcite amount and Ca/Al ratio as proxies for paleoproductivity (see paragraph 5.2).

The reliability of oxygen isotopes and calcareous plankton assemblages, allowed Addante et al. (2024) to apply the orbital tuning proposed by Hilgen (1991a) and the comparison with other reference curves (Grant et al., 2022; Bolton et al., 2010). Among these, the obliquity and insolation curves (Laskar et al., 2004), and the 'LR04 stack' (Lisiecki and Raymo, 2005; Ahn et al., 2017), are reported in Fig. 4 in correlation with the $MSN_{t\text{-}s}$ isotope curves. The not perfect alignment of the LR04 stack with the $MSN_{t\text{-}s}$ curves depends on the time lag applied and the age model proposed. Fig. 4 also reports the sea level curves proposed by Jakob et al. (2020) and Miller et al. (2020) in which the large fluctuations during the MIS G4, G2 and 104 are strongly correlated with those of the LR04 stack. This is despite the fact that the two sea level curves show differences greater than 40 m. This correlation highlights that, at global level, the obliquity forcing controls the bottom waters and the sea level variations. Conversely, in the Mediterranean Sea surface temperatures and circulation patterns (see paragraph 5.3) are mainly influenced by the precession/insolation cycles, as also already described by Grant et al. (2022) and Addante et al. (2024). Obviously, the obliquity signal also interferes with insolation by amplifying its effects when it is in phase, and mitigating the same when it is opposite. In particular, at the $MSN_{t\text{-}s}$ heavier $\delta^{18}O$ values are documented in the MIS 104, G2, and G4 in correspondence with obliquity minima (Fig. 4). In addition, the isotopic signal is also strongly influenced by the insolation with the lowest $\delta^{18}O$ values coinciding with the highest TOC contents. At last, lithology, chromatic variations and TOC are exclusively controlled by insolation, with darker colours and higher organic content correlating with insolation maxima. As for the depth profile of $\delta^{13}C_{bulk}$ over time, it shows a weak cyclical trend, with a slight lowering of $\delta^{13}C$ occurred in all sapropels with the exception of sapropel A3, where no significant variations have been recorded. Conversely, a strong excursion towards lower values (~−0.8‰) coincides with the A5 ^{12}C enrichments, also characterizing the underlying marls deposited during MIS 104. A similar decrease was measured in $\delta^{13}C_{Uvigerina\ spp}$ by Zanola et al. (2024) from the nearby "Mandorlo" section. It testifies an organic carbon contribution probably related to the local currents dynamic as better illustrated in paragraph 5.3.

5.2. Paleoenvironmental reconstruction

In order to define the paleoenvironmental conditions during the deposition of the studied interval, a reduced number of geochemical proxies has been selected and reported with respect to the obliquity and insolation curves (Laskar et al., 2004) (Fig. 5).

According to Beltran et al. (2007), who link carbonate content to foraminifera and coccolith remains, and as confirmed by Addante et al. (2024), in the studied section the Ca/Al ratio (likewise the $CaCO_3$ and calcite content) assumes the role of a paleoproductivity indicator. At the same time, the organic matter decomposition produces the enrichment of the bottom water in phosphorus (and in other nutrient elements) which passes into solution in the form of PO_4^{3-}. The upwelling of these nutrient-rich bottom waters (mainly the LIW, see paragraph 5.3) further promotes the surface productivity and, depending on the conditions, the preservation of phosphorus in sediments, being adsorbed on oxy-hydroxides or forming authigenic apatite (Tribovillard et al., 2006; Scopelliti et al., 2010). As a consequence, phosphorus gives indication both on enhanced sea surface fertility and active water column circulation. In the $MSN_{t\text{-}s}$, Ca/Al and P/Al show the same trend, with higher values in the marly levels, which is also synchronous with that of the Hydrogen Index. This is in agreement with the higher H/C ratio characterizing the marine organic matter, enriched in lipids and proteins, compared to the carbohydrate-rich constituents of land plants. As a consequence, an increase in HI indicates periods of enhanced marine productivity (Killops and Killops, 2013). More in detail, Fig. 5 shows that the productivity follows the insolation curve, only weakly subordinate to the influence of obliquity. It increases in the marls but a maximum of productivity is recorded when insolation minima coincide with obliquity maxima during G1 and G3. Conversely, when insolation minima coincide with obliquity minima the productivity is less pronounced.

The Ba/Al ratio, commonly used as a reference paleoproductivity

indicator, in the MSN_{t-s} shows a different pattern with respect to the above considered proxies, and is not comparable with the Ba/Al profile from the Eastern Mediterranean ODP Site 967 (Grant et al., 2022). As shown in Fig. 3, a clear relation with the lithology is lacking, this ratio being characterized by a wide increase in the marls between the sapropels A4 and A4/5 and two sharp peaks above the sapropels A2 and A3. Enrichments in barium just above anoxic levels are common and well known as "barium diagenetic fronts" (van Os et al., 1991, 1994; Torres et al., 1996). Barium, in fact, is generally fixed in sediments as barite ($BaSO_4$) but this mineral can be used as a final electron acceptor during the oxidation of organic matter as anoxic conditions prograde. As a result, barium is remobilized to re-precipitate where conditions are again oxygenated, forming oxidation fronts at the upper limits of sapropelic levels (McManus et al., 1998). For this reason the applicability of barium as paleoproductivity proxy is generally limited to oceanic settings characterized by well oxygenated bottom water (Pirrung et al., 2008; Schoepfer et al., 2015; Cutmore et al., 2023).

In the MSN_{t-s}, productivity variations are clearly related to the fluctuations in the continental inputs. In particular, as mentioned in section 4.4, titanium and zirconium are associated with eolian dust inputs, while potassium and rubidium to continental runoff. During humid periods, heavy minerals such as zircon, titanite and rutile, very resistant to alteration, tend to deposit in low-energy river stretches, forming fluvial placer deposits. During arid periods, their transport is tied to eolian contribution, constituting the Saharan eolian dust that is deposited in basins adjacent to northern Africa (Grant et al., 2022). Conversely, potassium and rubidium, mainly contained in illite and feldspars, increase during humid periods as also documented in different coeval sections (Punta Piccola, Monte Singa, and Vrica) and at ODP Site 964 A (Leg 160) (Foucault and Mélières, 2000). To summarize the antagonism between the riverine and eolian contribution the Rb/Zr ratio has been reported in Fig. 5. The high productivity marl levels are characterized by decrease in Rb/Zr ratio, corresponding to insolation minima and deposited during cold and arid periods, whilst higher values occur in sapropels during insolation maxima and deposited in warm/-humid periods. The increases in runoff inputs during the deposition of the sapropels is also confirmed by lower $\delta^{18}O$ values (Fig. 4) and higher percentages in clay minerals (Fig. 5).

Quartz shows an anomalous trend with an increase upwards from A4 to A5 and peaks in the sapropels. Although quartz is a mineral associated with eolian dust (Foucault and Mélières, 2000) in the MSN_{t-s} it increases during the insolation maxima related to more humid conditions and increased runoff. Nevertheless, focussing on the marl levels during MIS 104 and G2, considered as cool periods and linked to obliquity and insolation minima, a smaller decrease in quartz abundance is documented, that may be related to the sea level falls and greater contribution of eolian dust from northern Africa.

The documented increase in freshwater inputs during insolation peaks is therefore closely related to the formation of sapropels, as widely described (Rossignol-Strick, 1983, Vergnaud-Grazzini, 1985; deMenocal and Tierney, 2012; Larrasoaña et al., 2013; Plancq et al., 2015; Grant et al., 2017), causing the establishment of a strong water column stratification. Actually, all redox-sensitive elements well mark the sapropels, but not all in the same way. To well detail the magnitude of anoxia among the five investigated sapropels, the "redox ladder" proposed by Grundl et al. (2011) and modified by Algeo and Li (2020), in which the thresholds for specific redox couples are illustrated (Fig. 6), is here considered. In this scale, the upper limit of the suboxic zone is defined by the NO_3^-/N_2 couple and the lower one by the SO_4^{2-}/H_2S couple. The suboxic zone is further subdivided by the MnO_2/Mn^{2+} couple into a "suboxidized zone" having very low dissolved O_2 concentrations and a "subreduced zone" containing no dissolved O_2 or H_2S. An important reaction relative to the Fe^{3+}/Fe^{2+} couple characterize the upper subreduced zone. Iron, being involved in the reduction reaction at lower Eh, passes to the divalent state Fe^{2+} that, if the conditions become euxinic (SO_4^{2-}/H_2S transition), binds to the reduced sulfur precipitating as pyrite.

In the MSN_{t-s} nickel, as well as copper and zinc, shows clear enrichments in all the sapropels (Fig. 5). These elements besides entering into the iron sulfides or forming their own sulfides under euxinic conditions, are preserved in sediment also under dysoxic/suboxic conditions through the formation of organo-metallic complexes (Morse and Luther, 1999). As a consequence, their enrichment does not permit to distinguish the extent of the decrease in Eh (Fig. 6).

Conversely, the Fe/Al ratio shows significant enrichments only in the sapropels A4/5 and A5, testifying pyrite precipitation and allowing to

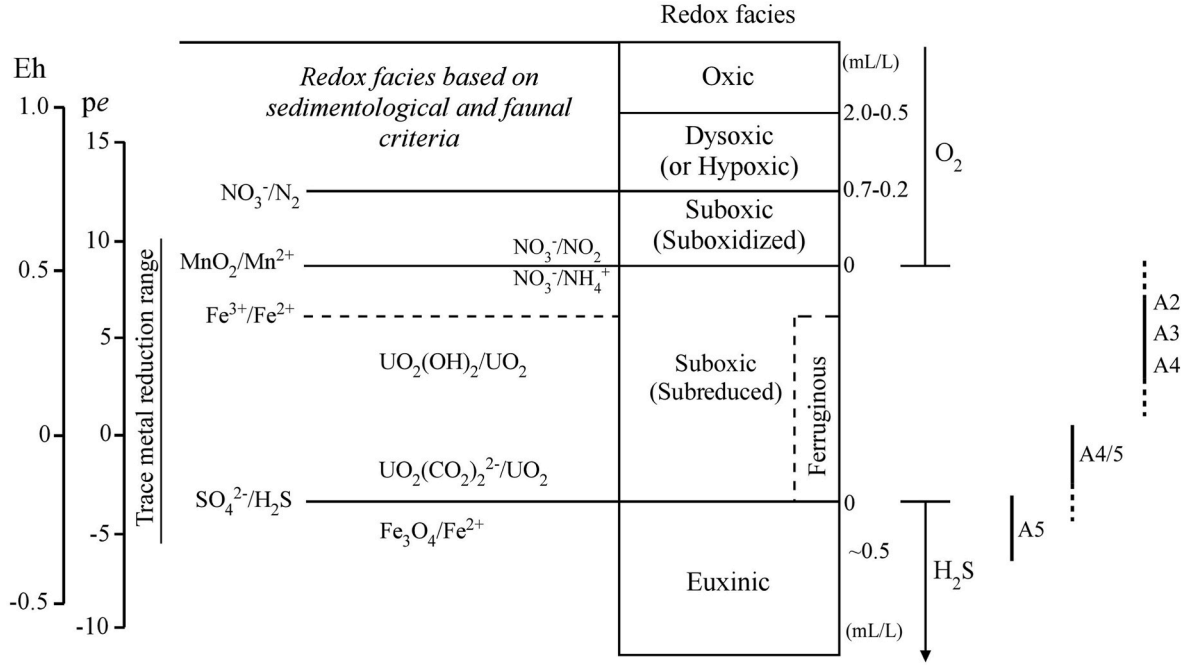

Fig. 6. Redox ladder of the main redox condition proxies modified from Algeo and Li (2020). On the right the deposition redox facies of the studied MSN sapropels (see text).

associate the deposition of these levels to euxinic conditions (Fig. 5). The capacity of cobalt to form a sulfide in solid solution with FeS_2 accounts for the same trend recorded by Co/Al (Tribovillard et al., 2006).

Further detail can be achieved taking into account the complementary geochemical behaviour of iron and manganese. The manganese oxides and hydroxides are involved in the oxidation of organic matter in the suboxic zone (Fig. 6) resulting in the reduction of Mn^{4+} to Mn^{2+} which, being much more soluble, quickly passes in solution causing manganese depletion in sediments. It is common that these minerals precipitate again when redox conditions return oxidizing, generally near or below the redox boundary (chemocline), resulting in manganese-enriched levels similar to what above described for the barium (Tribovillard et al., 2006). The last mechanism is probably responsible for the two sharp peaks recognized in the Mn/Al profile inside the sapropel A4 and at the top of the sapropel A2 (Fig. 3).

Given the opposite behaviour of iron and manganese, the Fe/Mn ratio (Figs. 5 and 6) may indicate suboxic conditions when moderate increases are purely determined by the dissolution of manganese oxy-hydroxides, is this the case of sapropels A2, A3, and A4, and euxinic conditions when the increases in Fe/Mn values are amplified by the precipitation of the iron as pyrite, as well as in sapropel A5 and, partially, A4/5.

Actually, only the sapropel A5 seems to exhibit fully euxinic conditions as also confirmed by TOC and U/Al profile (Figs. 4 and 5). Both the last indicators mark the sapropel A5 with a pronounced positive excursion. In particular, regarding the uranium, its preservation in the sediments as UO_2 is subordinated to the reduction from U^{6+} to U^{4+}. The change in the oxidation state is catalysed by the sulphate-reducing bacteria, therefore under euxinic conditions (Fig. 6) (Klinkhammer and Palmer, 1991; Brumsack, 2006; Scopelliti et al., 2006; Zhengji, 2010). The U/Al pattern, coupled with the Fe/Mn and TOC ones, allows to discriminate two different degrees of anoxia, subreduced-partially euxinic associated with the sapropel A4/5, and fully euxinic characterizing the sapropel A5.

The above fits well with the lithological evidence, documented by Radmacher et al. (2023) and Addante et al. (2024), that the sapropel A5 is the only one showing evident lamination, even if in the lowermost part of the Nb.

5.3. Paleogeographic and paleoceanographic reconstruction

The data presented in this study, and the paleoenvironment

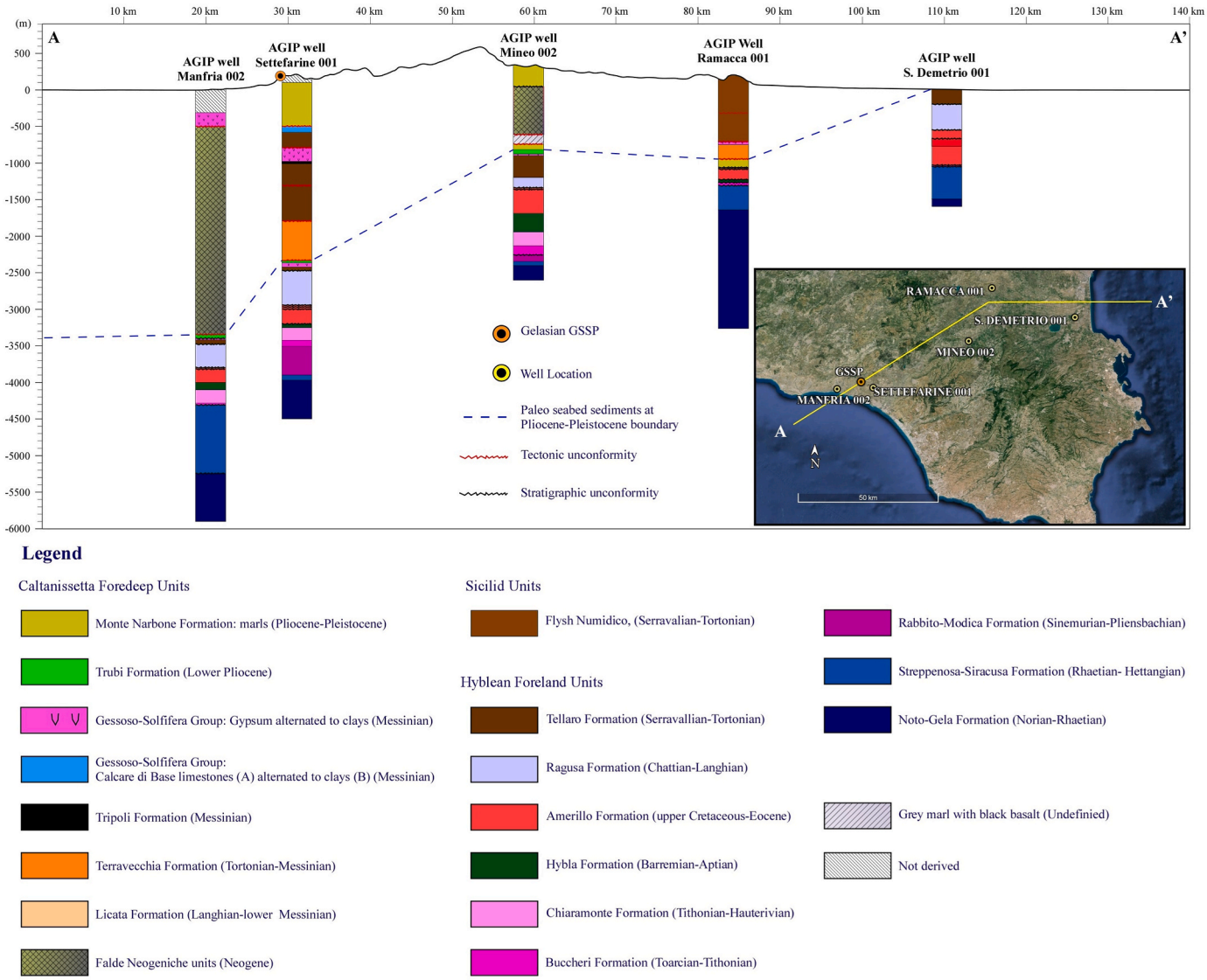

Fig. 7. Sedimentary logs and locations, with respect to the current topographic profile (trace A-A′), of the Manfria, Settefarine, Mineo, Ramacca, and S. Demetrio AGIP petroleum wells illustrating the stratigraphic sequences in the studied area (see text).

conditions characterizing the marl/sapropel couplets above described, permit to attempt the reconstruction of the possible paleogeographic context within which the $MSN_{t\text{-}s}$ was deposited.

The deposition of the Monte Narbone Fm. took place between the units of the Sicilian Appenninic-Maghrebian chain and the Hyblean foreland (Fig. 1), representing a basin within the Gela foredeep. From a tectonic point of view, the paleogeography of the studied area during the interval considered was predominantly conditioned by the opening of the Vavilov Basin (Vav. Basin) (Savelli and Ligi, 2017) to the North-Northwest and the advancement of the European crystalline units (Eu units) (Gueguen et al., 1998) towards the South-Southeast. This period was also characterized by a transition from predominantly thin-skinned to thick-skinned tectonics (Pfiffner, 2006), causing an interruption in the movement towards the foreland of the Sicilian chain, and a change in the deformation pattern that caused the onset of strong uplift in the late Gelasian-early Calabrian (Gasparo Morticelli et al., 2015). Although the persistent tectonic and volcanic activity of the area makes difficult estimating the exact position of the $MSN_{t\text{-}s}$ deposition areas, the identification of some structural units are documented by a series of seismic profiles and reconstructions from well-core data (Torelli et al., 1998) (Fig. 7). Structures such as the Ramacca-San Demetrio high were submerged elevated zones that separated the deep Ionian basin from the internal basin, located just in front of the chain. Further, the geological maps (Lentini et al., 2009, 2010; Carbone et al., 2011) show the presence of Pliocene-Pleistocene lithologies typical of a transition system between fluvial and inner/outer shelf, mainly composed by silty-clays and sands with mollusc fauna typical for shallow waters.

Based on these premises, a paleogeographic model during the Plio-Pleistocene transition is here presented, in which four structural units can be described (Fig. 8). The first one consists of a wide continental shelf characterized by predominantly Mesozoic-Cenozoic carbonate rocks more than 2000 m thick, known as Hyblean-Maltese platform

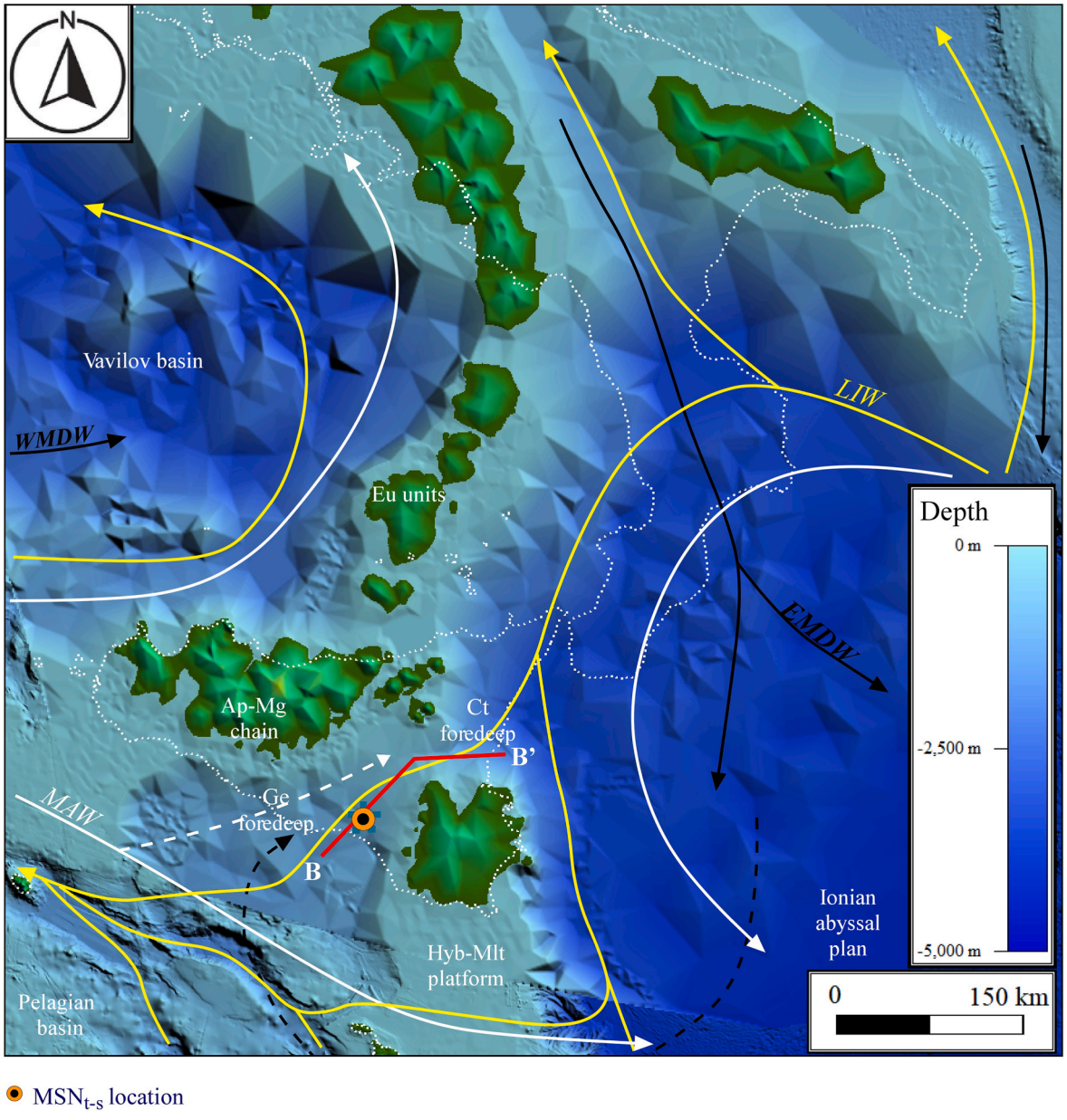

Fig. 8. Paleogeographic and paleocirculation reconstruction of the studied area referred to 2.6 Ma. White thin dashed lines: current geography; EU: European; Ap-Mg: Appenninic-Maghrebian; Ge: Gela; Ct: Catania; Hyb-Mlt: Hyblean-Maltese; white arrows: MAW (Modified Atlantic Water); yellow arrows: LIW (Levantine Intermediate Water); black arrows: WMDW and EMDW (Western and Eastern Mediterranean Deep Water, respectively); B-B′ red line: section of profiles represented in Fig. 9.

(Jongsma et al., 1985; Bishop and Debono, 1996; Schmitt et al., 2021) It is characterized by some emerged areas with a steep slope to the East in the Malta escarpment, while to the South and West, the transition to deep zones is more gradual (Torelli et al., 1998). The second one is the Sicilian Appenninic-Maghrebian (Ap-Mg) chain located in the North-West. It is characterized by numerous emerged areas and several thrust-top basins, some of which are deeper than 500 m. During the Plio-Pleistocene, those emerged areas were surrounded by a series of deltaic systems with drainage also towards the basin hosting the $MSN_{t\text{-}s}$ (Basilone, 2018; Dominici et al., 2020). The third paleogeographic domain is the Pelagian basin in the South-West. It represents a deep basin separated from the basin hosting the studied section by a system of horsts and grabens (Klett, 2001; Gasparo Morticelli et al., 2015; Maiorana et al., 2023). Finally, the Catania (Ct) foredeep, located in the North-East. It accounts of an area separated from the Gela (Ge) foredeep by a submerged structural high, tectonically active during the early

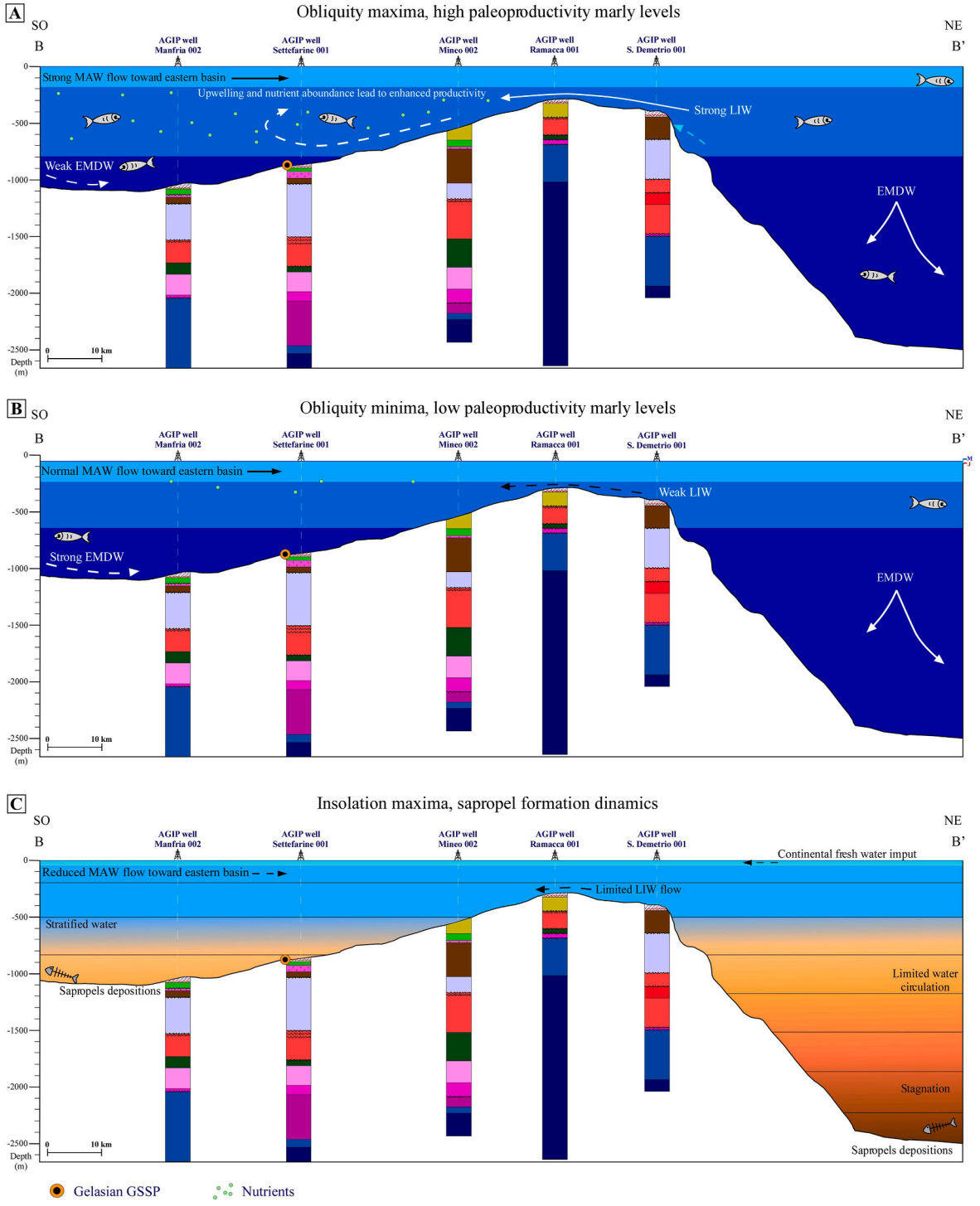

Fig. 9. Paleoenvironmental reconstruction at 2.6 Ma of the basin conditions during the deposition of marls and sapropels of the cluster A from the $MSN_{t\text{-}s}$. Three paleobathymetric profiles are shown according to the B-B′ section reported in Fig. 8: A) deposition of marly levels related to insolation minima and obliquity maxima (MIS G3 and G1); B) deposition of marly levels related to insolation and obliquity minima (MIS G2 and 104); C) deposition of sapropels during periods of insolation maxima (see text for details). Lithology of the well-core as in Fig. 7; MAW, LIW and EMDW as in Fig. 8.

Gelasian, characterized by highly varied sedimentation. The sediments that constitute it, appear today to be disturbed by numerous tectonic movements characterized by magmatic activity and gravitational phenomena (Torelli et al., 1998). Fig. 8 also shows the pattern of currents in the Central-Southern Mediterranean, contextualized within the reconstructed paleogeography. The reconstruction of surface, intermediate, and deep currents has been made assuming that the Mediterranean currents have remained largely unchanged until today (Cutmore et al., 2023), although with slight differences due to the palaeographic conformation of the Caltanissetta foredeep.

The deposition area of the $MSN_{t\text{-}s}$ was likely located in the Southwest portion of a structural high that separated the Gela foredeep from the Catania foredeep. This was determined by the convergence of the Sicilian chain front with the Hyblean foreland (Fig. 8). At the same time, this structural high can be considered as a sill controlling the water exchanges between the two basins and limiting the flow of the Levantine Intermediate Water (LIW), in particular during the sea level drops triggered by cool periods.

This particular paleogeographic context makes the basin particularly susceptible to cyclical orbital variations. During the deposition of marls related to insolation minima and obliquity maxima (MIS G3 and G1) the LIW flowed across the sill producing a strengthening of the paleocirculation. This resulted in mixing of the water column with potential upwelling of nutrients which added to those transported by the LIW from the northeast, producing the rise in paleoproductivity and decrease in the deposition of clay minerals hindered by bottom currents (Figs. 5 and 9A). Paleoproductivity increase was less pronounced during MIS G2 and 104 linked to insolation and obliquity minima (Fig. 5). This latter was probably due to a slowdown of the LIW caused by both lower insolation and by the sea level draw down (Fig. 9B) as suggested by the correlation with the sea level curves proposed by Jakob et al. (2020) and Miller et al. (2020) reported in Fig. 4.

The marls of MIS 104 are also characterized by anomalous lighter $\delta^{13}C_{bulk}$ values (Fig. 5), also recorded in the $\delta^{13}C_{\textit{Uvigerina spp}}$ by Zanola et al. (2024). This excursion may be the result of the contribution of the organic carbon recycling from underlying sapropel (A4/5) in response to a LIW slowdown. Alternatively, the lighter $\delta^{13}C$ values may be due to the reinforcement of the Eastern Mediterranean Deep Water (EMDW), which caused the passage through the Malta escarpment of "old" and stagnant waters, previously trapped in the Ionian abyssal plain, driven by "new" and colder bottom waters formed during MIS 104 (Fig. 9B). In this scenario, the EMDW became particularly dense during cold periods (i.e. MIS 104) and underwent enhanced circulation. This increased density would have been a result of lower surface temperatures and enhanced salinity due to higher evaporation rates during cold and arid climatic phases. The denser water would sink more efficiently, leading to stronger bottom currents. As these denser waters accumulated in deeper parts of the basin, the hydrostatic pressure would have increased, essentially "pushing up" the older, stagnant deep waters that were previously isolated in the abyssal plains. This upward displacement, or shoaling of the deep water mass, allowed the stagnant deep waters to rise higher in the water column. Once these deep waters became shallower, they were able to spill over topographic barrier like the Malta escarpment, enabling their entry into shallower basins such as in the Gela foredeep. This process occurred during periods of strong climatic cooling, when enhanced bottom water formation intensifies deep-water circulation and redistributes water masses across adjacent basins. Both hypotheses' accounts for slight variations in some redox proxies. Actually, although the marls were formed under oxic condition, MIS G2 and 104 show moderate increases in the Fe/Mn ratio (Fig. 5), which may also indicate reduced paleocirculation and reduced mixing in the sea water column (Żarczyński et al., 2019).

On the contrary, during periods of insolation maxima, the northward migration of the Intertropical Convergence Zone caused the establishment of humid conditions with consequent increase in the continental runoff from North Africa and formation of a freshwater surface layer (Fig. 9C). These conditions are marked in the $MSN_{t\text{-}s}$ by lower values in $\delta^{18}O_{bulk}$, and increases in the Rb/Zr ratio and in abundance of clay minerals (Figs. 4 and 5). Moreover, the higher abundance of quartz and feldspars in the sapropels (Fig. 5 and Table 1) suggests a significant contribution from the emerged areas of the Sicilian Appenninic-Maghrebian chain and the Hyblean foreland.

The consequent water stratification, and the formation of variable dysoxic to euxinic environments, are supported by all the above described redox proxies and by the partial dissolution in the sapropels of coccoliths in the nannoplankton assemblages, as reported by Addante et al. (2024).

In this scenario, the sapropel A5 (Nb; i-250) differs from the others, with Fe/Mn and U/Al ratios giving evidence of deposition under fully euxinic and water-stagnation conditions. Actually, according to Radmacher et al. (2023) and Addante et al. (2024), the Nb is the only sapropel showing a clear laminations, at least in its lowermost portion.

6. Conclusion

The geochemical and mineralogical data investigated at the $MSN_{t\text{-}s}$ reveal a depositional system particularly sensitive to global climatic variations induced by astronomical forcing during the late Pliocene and early Pleistocene.

By comparing our data with an original paleogeographic context, we propose a depositional setting subject to terrigenous inputs from the surrounding emerged areas and deep water influxes changing in response both insolation and obliquity cycles. In particular, runoff and anoxia were primarily associated with insolation cycles, whilst paleoproductivity and paleocurrents were linked to obliquity cycles with a stronger intensification of deep water influxes and nutrients upwelling occurred during periods of obliquity maxima.

According to our scenario, the upwelling processes characterizing the marls deposition were developed during the insolation minima but with an influence of the obliquity. More in detail, the upwelling current were more marked during the obliquity maxima (G1 and G3) when the LIW flowed across the sill from the Ionian basin, producing a strengthening of the paleocirculation. On the contrary, during the obliquity minima, and in particular in the cold and arid MIS 104, the EMDW became particularly dense strengthening the bottom current. These cold denser waters pushed up the older stagnant deep waters accumulated in the Ionian basin favouring the crossing of the Malta escarpment. It activated a less marked deep water upwelling in the Gela foredeep.

Conversely, during the insolation maxima the increase in the continental runoff produced a strong water stratification, weakening the LIW, and causing the sapropels formation. Also the redox conditions at the seafloor were not the same during the deposition of the sapropels A2–A5. In fact, anoxic conditions were gradually more restricted passing from the sapropels A2, A3 and A4, deposited under suboxic conditions, to the sapropels A4/5 and A5 characterized by deposition under subreduced and euxinic conditions, respectivelly. Actually, the development of fully euxinic environments only characterize the sapropel A5 (Nb).

CRediT authorship contribution statement

Stefano Fasone: Writing – review & editing, Writing – original draft, Visualization, Software, Methodology, Investigation, Data curation, Conceptualization. **Giovanna Scopelliti:** Writing – review & editing, Supervision, Methodology, Investigation, Funding acquisition, Data curation. **François Baudin:** Writing – review & editing, Methodology, Formal analysis. **Antonio Caruso:** Writing – review & editing, Supervision, Project administration, Investigation, Funding acquisition, Conceptualization.

Declaration of competing interest

The authors declare that they have no known competing financial interests or personal relationships that could have appeared to influence the work reported in this paper.

Data availability

Data will be made available on request.

Acknowledgements

This research is part of the GELSTRAT project, an international cooperation sponsored by INQUA-SACCOM-SQS and aimed for re-studying the Gelasian Stage GSSP. It also falls in the REMEPP project funded by Italian PRIN PNRR 2022 (responsible A. Caruso). Financial support for the geochemical analysis performed at the ActLabs Ltd and for a research grant at SF has been provided by UNIPA FFR 2023/2024 grants (responsible G. Scopelliti). The authors thank M. Addante, A. Bertini, A. Girone, M. Head, P. Maiorano, M. Marino, R. Radmacher for the discussions we had during our collaboration for the study of the Gelasian GSSP. The authors are indebted to the anonymous reviewers for their valuable comments that greatly improved the manuscript.

References

Addante, M., Maiorano, P., Scopelliti, G., Girone, A., Marino, M., Trotta, S., Caruso, A., 2024. Climate-induced surface water variability at Monte san Nicola type-section (sicily, southern Italy): new data across the gelasian GSSP. Palaeogeogr. Palaeoclimatol. Palaeoecol. 634, 111907. https://doi.org/10.1016/j.palaeo.2023.111907.

Ahn, S., Khider, D., Lisiecki, L.E., Lawrence, C.E., 2017. A probabilistic Pliocene–Pleistocene stack of benthic $\delta^{18}O$ using a profile hidden Markov model. Dynamics and Statistics of the Climate System 2 (1), dzx002. https://doi.org/10.1093/climsys/dzx002.

Algeo, T.J., Li, C., 2020. Redox classification and calibration of redox thresholds in sedimentary systems. Geochem. Cosmochim. Acta 287, 8–26. https://doi.org/10.1016/j.gca.2020.01.055.

Bartoli, G., Sarnthein, M., Weinelt, M., Erlenkeuser, H., Garbe-Schönberg, D., Lea, D.W., 2005. Final closure of Panama and the onset of northern hemisphere glaciation. Earth Planet Sci. Lett. 237, 33–44. https://doi.org/10.1016/j.epsl.2005.06.020.

Basilone, L., 2018. Lithostratigraphy of Sicily. Springer, Heidelberg. https://doi.org/10.1007/978-3-319-73942-7.

Baudin, F. (Ed.), 2024. The Rock-Eval Method: Principles and Application. John Wiley & Sons.

Becker, J., Lourens, L.J., Hilgen, F.J., Van Der Laan, E., Kouwenhoven, T.J., Reichart, G.-J., 2005. Late Pliocene climate variability on Milankovitch to millennial time scales: a high-resolution study of MIS100 from the Mediterranean. Palaeogeogr. Palaeoclimatol. Palaeoecol. 228, 338–360. https://doi.org/10.1016/j.palaeo.2005.06.020.

Behar, F., Beaumont, V.D.E.B., Penteado, H.D.B., 2001. Rock-Eval 6 technology: performances and developments. Oil Gas Sci. Technol. 56 (2), 111–134.

Beltran, C., De Rafélis, M., Minoletti, F., Renard, M., Sicre, M.A., Ezat, U., 2007. Coccolith $\delta^{18}O$ and alkenone records in middle Pliocene orbitally controlled deposits: high-frequency temperature and salinity variations of sea surface water. G-cubed 8, 2006GC001483. https://doi.org/10.1029/2006GC001483.

Beltran, C., Sicre, M.-A., Ohneiser, C., Sainz, M., 2021. A composite Pliocene record of sea surface temperature in the central Mediterranean (Capo Rossello composite section – south Sicily). Sediment. Geol. 420, 105921. https://doi.org/10.1016/j.sedgeo.2021.105921.

Bishop, W.F., Debono, G., 1996. The hydrocarbon geology of Southern offshore Malta and surronding regions. J. Petrol. Geol. 19, 129–160. https://doi.org/10.1111/j.1747-5457.1996.tb00422.x.

Bolton, C.T., Wilson, P.A., Bailey, I., Friedrich, O., Beer, C.J., Becker, J., Baranwal, S., Schiebel, R., 2010. Millennial-scale climate variability in the subpolar North Atlantic ocean during the late Pliocene. Paleoceanography 25 (4). https://doi.org/10.1029/2010PA001951.

Brumsack, H.-J., 2006. The trace metal content of recent organic carbon-rich sediments: implications for Cretaceous black shale formation. Palaeogeogr. Palaeoclimatol. Palaeoecol. 232, 344–361. https://doi.org/10.1016/j.palaeo.2005.05.011.

Capraro, L., Bonomo, S., Di Stefano, A., Ferretti, P., Fornaciari, E., Galeotti, S., Incarbona, A., Macrì, P., Raffi, I., Sabatino, N., Speranza, F., Sprovieri, M., Di Stefano, E., Sprovieri, R., Rio, D., 2022. The Monte san Nicola section (sicily) revisited: a potential unit-stratotype of the gelasian stage. Quat. Sci. Rev. 278, 107367. https://doi.org/10.1016/j.quascirev.2021.107367.

Carbone, S., Lentini, F., Scribano, V., Ruggeri, R., Maniscalco, R., Marino, M., 2011. Carta Geologica d'Italia alla scala 1:50000 del foglio 641 Augusta. Progetto CARG. ISPRA, S.EL.CA. Firenze.

Caruso, A., 2004. Climatic changes during late Pliocene and early Pleistocene at Capo Rossello (Sicily, Italy): response from planktonic foraminifera. In: Proceedings of the First Italian Meeting on Environmental Micropaleontology, vol. 9. Grzybowski Foundation Special publication, pp. 17–36.

Castradori, D., Rio, D., Hilgen, F.J., Lourens, L.J., 1998. The global standard stratotype-section and point (GSSP) of the piacenzian stage (middle Pliocene). Episodes 21, 88–93.

Catalano, R., Valenti, V., Albanese, C., Accaino, F., Sulli, A., Tinivella, U., Gasparo Morticelli, M., Zanolla, C., Giustiniani, M., 2013. Sicily's fold–thrust belt and slab roll-back: the SI.RI.PRO. seismic crustal transect. J. Geol. Soc. 170 (3), 451–464. https://doi.org/10.1144/jgs2012-099.

Channell, J.E.T., Di Stefano, E., Sprovieri, R., 1992. Calcareous plankton biostratigraphy, magnetostratigraphy, and paleoclimatic history of the Plio-Pleistocene Monte S. Nicola section (Southern Sicily). Bollettino Società Paleontologica Italiana 31, 351–382.

Cita, M.B., Capraro, L., Ciaranfi, N., Stefano, E.D., Lirer, F., Maiorano, P., Marino, M., Raffi, I., Rio, D., Sprovieri, R., Stefanelli, S., Vai, G.B., 2008. The calabrian stage redefined. Episodes 31, 408–419. https://doi.org/10.18814/epiiugs/2008/v31i4/006.

Cutmore, A., Bale, N., De Lange, G.J., Nijenhuis, I.A., Lourens, L.J., 2023. A window into eastern mediterranean productivity conditions over three Pliocene precession-forced climate cycles. Paleoceanogr. Paleoclimatol. 38, e2022PA004550. https://doi.org/10.1029/2022PA004550.

Dymond, J., Suess, E., Lyle, M., 1992. Barium in deep-sea sediment: a geochemical proxy for paleoproductivity. Paleoceanography 7 (2), 163–181. https://doi.org/10.1029/92PA00181.

deMenocal, P.B., Tierney, J.E., 2012. Green Sahara: african humid periods paced by earth's orbital changes. Nature Education Knowledge 3 (10), 12.

Dickson, J.A.D., Coleman, M.L., 1990. Changes in carbon and oxygen isotope composition during limestone diagenesis. In: Tucker, M.E., Bathurst, R.G.C. (Eds.), Carbonate Diagenesis. Wiley, pp. 259–270. https://doi.org/10.1002/9781444304510.ch21.

Dominici, S., Benvenuti, M., Garilli, V., Uchman, A., Pollina, F., David, A., 2020. Pliocene-Pleistocene stratigraphic paleobiology at Altavilla Milicia (Palermo, Sicily): tectonic, climatic and eustatic forcing (other). Bollettino Società Paleontologica Italiana 59, 57–83. https://doi.org/10.5194/egusphere-egu2020-9271.

Emeis, K.C., Robertson, A.H.F., Richter, C., 1996. Paleoceanography and sapropel introduction. In: Proceedings of the Ocean Drilling Program, Initial Reports, vol. 160, pp. 21–28.

Emeis, K.C., Struck, U., Schulz, H.M., Rosenberg, R., Bernasconi, S., Erlenkeuser, H., Sakamoto, T., Martinez-Ruiz, F., 2000. Temperature and salinity variations of Mediterranean Sea surface waters over the last 16,000 years from records of planktonic stable oxygen isotopes and alkenone unsaturation ratios. Palaeogeogr Palaeocl 158, 259–280. https://doi.org/10.1016/S0031-0182(00)00053-5.

Emeis, K.C., Schulz, H., Struck, U., Rossignol-Strick, M., Erlenkeuser, H., Howell, M.W., Kroon, D., Mackensen, A., Ishizuka, S., Oba, T., Sakamoto, T., Koizumi, I., 2003. Eastern Mediterranean surface water temperatures and δ18O composition during deposition of sapropels in the late Quaternary. Paleoceanography 18, 1005. https://doi.org/10.1029/2000PA000617.

Foucault, A., Mélières, F., 2000. Palaeoclimatic cyclicity in central Mediterranean Pliocene sediments: the mineralogical signal. Palaeogeogr. Palaeoclimatol. Palaeoecol. 158, 311–323. https://doi.org/10.1016/S0031-0182(00)00056-0.

Gasparo Morticelli, M., Valenti, V., Catalano, R., Sulli, A., Agate, M., Avellone, G., Albanese, C., Basilone, L., Gugliotta, C., 2015. Deep controls on foreland basin system evolution along the Sicilian fold and thrust belt. Bull. Soc. Geol. Fr. 186, 273–290. https://doi.org/10.2113/gssgfbull.186.4-5.273.

Gibbard, P.L., Head, M.J., 2010. The newly-ratified definition of the Quaternary System/Period and redefinition of the Pleistocene Series/Epoch, and comparison of proposals advanced prior to formal ratification. Episodes Journal of International Geoscience 33 (3), 152–158.

Gibbard, P.L., Head, M.J., Walker, M.J.C., the Subcommission on Quaternary Stratigraphy, 2010. Formal ratification of the quaternary system/period and the Pleistocene series/epoch with a base at 2.58 Ma. J. Quat. Sci. 25 (2), 96–102. https://doi.org/10.1002/jqs.1338.

Grant, K.M., Rohling, E.J., Westerhold, T., Zabel, M., Heslop, D., Konijnendijk, T., Lourens, L., 2017. A 3 million year index for North African humidity/aridity and the implication of potential pan-African Humid periods. Quat. Sci. Rev. 171, 100–118. https://doi.org/10.1016/j.quascirev.2017.07.005.

Grant, K.M., Amarathunga, U., Amies, J.D., Hu, P., Qian, Y., Penny, T., Rodriguez-Sanz, L., Zhao, X., Heslop, D., Liebrand, D., Hennekam, R., Westerhold, T., Gilmore, S., Lourens, L.J., Roberts, A.P., Rohling, E.J., 2022. Organic carbon burial in Mediterranean sapropels intensified during Green Sahara Periods since 3.2 Myr ago. Communication Earth and Environment 3, 11. https://doi.org/10.1038/s43247-021-00339-9.

Gražulis, S., Chateigner, D., Downs, R.T., Yokochi, A.F.T., Quirós, M., Lutterotti, L., Manakova, E., Butkus, J., Moeck, P., Le Bail, A., 2009. Crystallography Open Database - an open-access collection of crystal structures. J. Appl. Crystallogr. 42, 726–729. https://doi.org/10.1107/S0021889809016690.

Grundl, T.J., Haderlein, S., Nurmi, J.T., Tratnyek, P.G., 2011. Introduction to aquatic redox chemistry. In: Tratnyek, P.G., Grundl, T.J., Haderlein, S.B. (Eds.), ACS Symposium Series. American Chemical Society, Washington, DC, pp. 1–14. https://doi.org/10.1021/bk-2011-1071.ch001.

Gueguen, E., Doglioni, C., Fernandez, M., 1998. On the post-25 Ma geodynamic evolution of the western Mediterranean. Tectonophysics 298, 259–269. https://doi.org/10.1016/S0040-1951(98)00189-9.

Haug, G.H., Tiedemann, R., 1998. Effect of the formation of the Isthmus of Panama on atlantic ocean thermohaline circulation. Nature 393, 673–676. https://doi.org/10.1038/31447.

Haug, G.H., Tiedemann, R., Zahn, R., Ravelo, A.C., 2001. Role of Panama uplift on oceanic freshwater balance. Geology 29, 207–210. https://doi.org/10.1130/0091-7613(2001)029<0207:ROPUOO>2.0.CO;2.

Henrichs, S.M., Reeburgh, W.S., 1987. Anaerobic mineralization of marine sediment organic matter: rates and the role of anaerobic processes in the oceanic carbon economy. Geomicrobiol. J. 5, 191–237. https://doi.org/10.1080/01490458709385971.

Herbert, T.D., Ng, G., Cleaveland Peterson, L., 2015. Evolution of Mediterranean sea surface temperatures 3.5–1.5 Ma: Regional and hemispheric influences. Earth Planet Sci. Lett. 409, 307–318. https://doi.org/10.1016/j.epsl.2014.10.006.

Hilgen, F.J., 1991a. Astronomical calibration of Gauss to matuyama sapropels in the mediterranean and implication for the geomagnetic polarity time scale. Earth Planet Sci. Lett. 104, 226–244. https://doi.org/10.1016/0012-821X(91)90206-W.

Hilgen, F.J., 1991b. Extension of the astronomically calibrated (polarity) time scale to the Miocene-Pliocene boundary. Earth Planet Sci. Lett. 107, 349–368. https://doi.org/10.1016/0012-821X(91)90206-W.

Jakob, K.A., Wilson, P.A., Pross, J., Ezard, T.H.G., Fiebig, J., Repschläger, J., Friedrich, O., 2020. A new sea-level record for the Neogene/Quaternary boundary reveals transition to a more stable East Antarctic Ice Sheet. In: Proceedings of the National Academy of Sciences, vol. 117, pp. 30980–30987. https://doi.org/10.1073/pnas.2004209117, 49.

Jongsma, D., van Hinte, J.E., Woodside, J.M., 1985. Geologic structure and neotectonics of the North african continental margin south of sicily. Mar. Petrol. Geol. 2, 156–179.

Kidd, R.B., Cita, M.B., Ryan, W.B.F., 1978. Stratigraphy of eastern Mediterranean sapropel sequences recovered during DSDP Leg 42A and their paleoenvironmental significance. In: Hsü, K.J., Montadert, L., et al. (Eds.), Initial Reports DSDP, vol. 42. U.S. Govt. Printing Office, Washington, pp. 421–443 (Pt. 1.

Killops, S.D., Killops, V.J., 2013. Introduction to Organic Geochemistry. John Wiley & Sons.

Klett, 2001. Total Petroleum Systems of the Pelagian Province, Tunisia, Libya, Italy, and Malta; the Bou Dabbous, Tertiary and Jurassic-Cretaceous Composite. U.S. Geological Survey Bulletin, pp. 2202–D. https://doi.org/10.3133/b2202D.

Klinkhammer, G., Palmer, M., 1991. Uranium in the oceans: where it goes and why. Geochem. Cosmochim. Acta 55, 1799–1806.

Lafargue, E., Marquis, F., Pillot, D., 1998. Rock-Eval 6 applications in hydrocarbon exploration, production, and soil contamination studies. Rev. Inst. Fr. Petrol 53 (4), 421–437.

Larrasoaña, J.C., Roberts, A.P., Rohling, E.J., 2013. Dynamics of green Sahara periods and their role in hominin evolution. PLoS One 8, e76514. https://doi.org/10.1371/journal.pone.0076514.

Laskar, J., Robutel, P., Joutel, F., Gastineau, M., Correia, A.C.M., Levrard, B., 2004. A long-term numerical solution for the insolation quantities of the Earth. Astron. Astrophys. 428, 261–285. https://doi.org/10.1051/0004-6361:20041335.

Lentini, F., Carbone, S., Cristofolini, R., Scamarda, G., Di Stefano, A., Corsaro, R.A., 2009. Carta Geologica d'Italia alla scala 1:50000 del foglio 634 Catania. Progetto CARG. ISPRA, S.EL.CA. Firenze.

Lentini, F., Carbone, S., Ferrara, V., Branca, S., Di Stefano, A., Romeo, M., Garfi, G., Pappalardo, G., 2010. Carta Geologica d'Italia alla scala 1:50000 del foglio 633 Paternò. Progetto CARG. ISPRA, S.EL.CA. Firenze.

Lentini, F., Carbone, S., 2014. Geologia della Sicilia - geology of sicily. Memorie Descr. Carta Geologica d'Italia 95, 7–414.

Lisiecki, L.E., Raymo, M.E., 2005. A Pliocene-Pleistocene stack of 57 globally distributed benthic $\delta^{18}O$ records. Paleoceanography 20. https://doi.org/10.1029/2004PA001071, 2004PA001071.

Liu, Z., Zhao, Y., Colin, C., Siringan, F.P., Wu, Q., 2009. Chemical weathering in Luzon, Philippines from clay mineralogy and major-element geochemistry of river sediments. Appl. Geochem. 24 (11), 2195–2205.

Lourens, L.J., Antonarakou, A., Hilgen, F.J., Van Hoof, A.A.M., Vergnaud-Grazzini, C., Zachariasse, W.J., 1996. Evaluation of the plio-pleistocene astronomical timescale. Paleoceanography 11, 391–413. https://doi.org/10.1029/96PA01125.

Lourens, L.J., Hilgen, F.J., Shackleton, N.J., Laskar, J., Wilson, D., 2004. The Neogene period. In: Gradstein, F. (Ed.), A Geologic Time Scale. Cambridge University Press, pp. 409–440.

Löwemark, L., Chen, H.-F., Yang, T.-N., Kylander, M., Yu, E.-F., Hsu, Y.-W., Lee, T.-Q., Song, S.-R., Jarvis, S., 2011. Normalizing XRF-scanner data: a cautionary note on the interpretation of high-resolution records from organic-rich lakes. J. Asian Earth Sci. 40, 1250–1256. https://doi.org/10.1016/j.jseaes.2010.06.002.

McManus, J., Berelson, W.M., Klinkhammer, G.P., Johnson, K.S., Coale, K.H., Anderson, R.F., Kumar, N., Burdige, D.J., Hammond, D.E., Brumsack, H.J., Mccorkle, D.C., Rushdi, A., 1998. Geochemistry of barium in marine sediments: implications for its use as a paleoproxy. Geochem. Cosmochim. Acta 62 (21–22), 3453–3473. https://doi.org/10.1016/S0016-7037(98)00248-8.

Maiorana, M., Artoni, A., Le Breton, E., Sulli, A., Chizzini, N., Torelli, L., 2023. Is the Sicily Channel a simple Rifting Zone? New evidence from seismic analysis with geodynamic implications. Tectonophysics 864, 230019. https://doi.org/10.1016/j.tecto.2023.230019.

Martinez-Ruiz, F., Kastner, M., Gallego-Torres, D., Rodrigo-Gámiz, M., Nieto-Moreno, V., Ortega-Huertas, M., 2015. Paleoclimate and paleoceanography over the past 20,000 yr in the Mediterranean Sea Basins as indicated by sediment elemental proxies. Quat. Sci. Rev. 107, 25–46. https://doi.org/10.1016/j.quascirev.2014.09.018.

Miller, K.G., Browning, J.V., Schmelz, W.J., Kopp, R.E., Mountain, G.S., Wright, J.D., 2020. Cenozoic sea-level and cryospheric evolution from deep-sea geochemical and continental margin records. Sci. Adv. 6, eaaz1346.

Morse, J.W., Luther, G.W., 1999. Chemical influences on trace metal-sulfide interactions in anoxic sediments. Geochem. Cosmochim. Acta 63, 3373–3378. https://doi.org/10.1016/S0016-7037(99)00258-6.

O'Dea, A., Lessios, H.A., Coates, A.G., Eytan, R.I., Restrepo-Moreno, S.A., Cione, A.L., Collins, L.S., De Queiroz, A., Farris, D.W., Norris, R.D., Stallard, R.F., Woodburne, M. O., Aguilera, O., Aubry, M.-P., Berggren, W.A., Budd, A.F., Cozzuol, M.A., Coppard, S.E., Duque-Caro, H., Finnegan, S., Gasparini, G.M., Grossman, E.L., Johnson, K.G., Keigwin, L.D., Knowlton, N., Leigh, E.G., Leonard-Pingel, J.S., Marko, P.B., Pyenson, N.D., Rachello-Dolmen, P.G., Soibelzon, E., Soibelzon, L., Todd, J.A., Vermeij, G.J., Jackson, J.B.C., 2016. Formation of the Isthmus of Panama. Sci. Adv. 2, e1600883. https://doi.org/10.1126/sciadv.1600883.

Ogniben, L., 1969. Schema introduttivo alla geologia del confine calabro-lucano, vol. 8. Memorie Società Geologica Italiana, pp. 453–763.

Pfiffner, O.A., 2006. Thick-skinned styles of continental contraction. In: Mazzoli, S., Butler, R.W.H. (Eds.), Styles of Continental Contraction, vol. 414. Geological Society of America Special Paper, pp. 153–177. https://doi.org/10.1130/2006.2414(09.

Pirrung, M., Illner, P., Matthießen, J., 2008. Biogenic barium in surface sediments of the European Nordic Seas. Mar. Geol. 250 (1–2), 89–103. https://doi.org/10.1016/j.margeo.2008.01.001.

Plancq, J., Grossi, V., Pittet, B., Huguet, C., Rosell-Melé, A., Mattioli, E., 2015. Multi-proxy constraints on sapropel formation during the late Pliocene of central Mediterranean (southwest Sicily). Earth Planet Sci. Lett. 420, 30–44. https://doi.org/10.1016/j.epsl.2015.03.031.

Radmacher, W., Head, M.J., Uchman, A., Mikołajczak, M., Lempart-Drozd, M., Kaczmarczyk, G.P., Wałachet, D., 2023. The Neogene–Quaternary boundary at its type locality, Monte San Nicola, Sicily, southern Italy: X-ray computed tomography and ichnofabric signals of the sapropelic Nicola bed. Mar. Petrol. Geol. 158, 106552.

Rio, D., Sprovieri, R., Stefano, E.D., 1994. The Gelasian Stage: a proposal of a new chronostratigraphic unit of the Pliocene series. Riv. Ital. Paleontol. Stratigr. 100 (1).

Rio, D., Sprovieri, R., Castradori, D., Stefano, E.D., 1998. The Gelasian Stage (Upper Pliocene): a new unit of the global standard chronostratigraphic scale. Episodes 21, 82–87. https://doi.org/10.18814/epiiugs/1998/v21i2/002.

Rohling, E.J., 1994. Review and new aspects concerning the formation of eastern Mediterranean sapropels. Mar. Geol. 122, 1–28. https://doi.org/10.1016/0025-3227(94)90202-X.

Rohling, E.J., Marino, G., Grant, K.M., 2015. Mediterranean climate and oceanography, and the periodic development of anoxic events (sapropels). Earth Sci. Rev. 143, 62–97. https://doi.org/10.1016/j.earscirev.2015.01.008.

Rollinson, H.R., 2014. Using Geochemical Data: Evaluation, Presentation, Interpretation. Routledge. https://doi.org/10.4324/9781315845548.

Rossignol-Strick, M., Nesteroff, W., Olive, P., Vergnaud-Grazzini, C., 1982. After the deluge: Mediterranean stagnation and sapropel formation. Nature 295, 105–110. https://doi.org/10.1038/295105a0.

Rossignol-Strick, 1983. African monsoons, an immediate climate response to orbital insolation. Nature 304, 46–49.

Savelli, C., Ligi, M., 2017. An updated reconstruction of basaltic crust emplacement in Tyrrhenian Sea, Italy. Nature Scientific Reports 7, 18024. https://doi.org/10.1038/s41598-017-17625-2.

Scheuvens, D., Schütz, L., Kandler, K., Ebert, M., Weinbruch, S., 2013. Bulk composition of northern African dust and its source sediments — a compilation. Earth Sci. Rev. 116, 170–194. https://doi.org/10.1016/j.earscirev.2012.08.005.

Schmidt, D.N., 2007. The closure history of the Central American seaway: evidence from isotopes and fossils to models and molecules. In: Williams, M., Haywood, A.M., Gregory, F.J., Schmidt, D.N. (Eds.), Deep-Time Perspectives on Climate Change: Marrying the Signal from Computer Models and Biological Proxies. Special Publications. https://doi.org/10.1144/TMS002.19. Geological Society of London. The Micropalentological Society.

Schmitt, T., Fritz, U., Delfino, M., Ulrich, W., Habel, J.C., 2021. Biogeography of Italy revisited: genetic lineages confirm major phylogeographic patterns and a pre-Pleistocene origin of its biota. Front. Zool. 18, 34. https://doi.org/10.1186/s12983-021-00418-9.

Schoepfer, S.D., Shen, J., Wei, H., Tyson, R.V., Ingall, E., Algeo, T.J., 2015. Total organic carbon, organic phosphorus, and biogenic barium fluxes as proxies for paleomarine productivity. Earth Sci. Rev. 149, 23–52. https://doi.org/10.1016/j.earscirev.2014.08.017.

Schrader, H., Matherne, A., 1981. Sapropel Formation in the eastern Mediterranean Sea: evidence from preserved opal assemblages. Micropaleontology 27, 191. https://doi.org/10.2307/1485285.

Scopelliti, G., Bellanca, A., Neri, R., Baudin, F., Coccioni, R., 2006. Comparative high-resolution chemostratigraphy of the bonarelli level from the reference bottaccione section (Umbria–Marche apennines) and from an equivalent section in NW sicily: consistent and contrasting responses to the OAE2. Chem. Geol. 228, 266–285. https://doi.org/10.1016/j.chemgeo.2005.10.010.

Scopelliti, G., Bellanca, A., Neri, R., Sabatino, N., 2010. Phosphogenesis in the Bonarelli Level from northwestern Sicily, Italy: petrographic evidence of microbial mediation and related REE behaviour. Cretac. Res. 31, 237–248. https://doi.org/10.1016/j.cretres.2009.11.004.

Sgarrella, F., Sprovieri, R., Di Stefano, E., Caruso, A., 1997. Paleoceanographic conditions at the base of the Pliocene in the southern Mediterranean basin. Riv. Ital. Paleontol. Stratigr. 103, 207–220.

Sprovieri, R., 1993. Pliocene-early Pleistocene astronomically forced planktonic foraminifera abundance fluctuations and chronology of Mediterranean calcareous plankton bio-events. Riv. Ital. Paleontol. Stratigr. 99 (3).

Sprovieri, R., Sprovieri, M., Caruso, A., Pelosi, N., Bonomo, S., Ferraro, L., 2006. Astronomic forcing on the planktonic foraminifera assemblage in the Piacenzian Punta Piccola section (southern Italy). Paleoceanography 21, PA4204. https://doi.org/10.1029/2006PA001268.

Thunell, R.C., Williams, G.D., 1982. The stepwise development of Pliocene-Pleistocene paleoclimatic and paleoceanographic conditions in the Mediterranean: oxygen isotopic studies of dsdp sites 125 and 132. Utrecht Micropaleontol. Bull. 30, 111–127.

Torelli, L., Grasso, M., Mazzoldi, G., Peis, D., 1998. Plio–quaternary tectonic evolution and structure of the Catania foredeep, the northern hyblean plateau and the ionian shelf (SE sicily). Tectonophysics 298, 209–221. https://doi.org/10.1016/S0040-1951(98)00185-1.

Torres, M.E., Brumsack, H.J., Bohrmann, G., Emeis, K.C., 1996. Barite fronts in continental margin sediments: a new look at barium remobilization in the zone of sulfate reduction and formation of heavy barites in diagenetic fronts. Chem. Geol. 127 (1–3), 125–139. https://doi.org/10.1016/0009-2541(95)00090-9.

Tribovillard, N., Algeo, T.J., Lyons, T., Riboulleau, A., 2006. Trace metals as paleoredox and paleoproductivity proxies: an update. Chem. Geol. 232, 12–32. https://doi.org/10.1016/j.chemgeo.2006.02.012.

van Os, B.J., Middelburg, J.J., de Lange, G.J., 1991. Possible diagenetic mobilization of barium in sapropelic sediment from the eastern Mediterranean. Mar. Geol. 100 (1–4), 125–136. https://doi.org/10.1016/0025-3227(91)90229-W.

van Os, B.J.H., Lourens, L.J., Beaufort, L., Hilgen, F.J., de Lange, G.J., 1994. The formation of Pliocene sapropels and carbonate cycles in the Mediterranean: diagenesis, dilution and productivity. Paleoceanography 9, 601–617. https://doi.org/10.1029/94PA00597.

Vergnaud-Grazzini, C., 1985. Mediterranean late cenozoic stable isotope record: stratigraphic and paleoclimatic implications. In: Stanley, D.J., Wezel, F.-C. (Eds.), Geological Evolution of the Mediterranean Basin: Raimondo Selli Commemorative Volume. Springer, New York, New York, NY, pp. 413–451. https://doi.org/10.1007/978-1-4613-8572-1_20.

Wehausen, R., Brumsack, H.-J., 2000. Chemical cycles in Pliocene sapropel-bearing and sapropel-barren eastern Mediterranean sediments. Palaeogeogr. Palaeoclimatol. Palaeoecol. 158, 325–352. https://doi.org/10.1016/S0031-0182(00)00057-2.

Zanola, E., Bonomo, S., Incarbona, A., Di Stefano, A., Distefano, S., Ferretti, P., Fornaciari, E., Galeotti, S., Macrì, P., Raffi, I., Sabatino, N., Speranza, F., Sprovieri, M., Di Stefano, E., Sprovieri, R., Rio, D., Capraro, L., 2024. High-resolution climate variability across the piacenzian/gelasian boundary in the Monte san Nicola section (sicily, Italy). Quat. Sci. Rev. 324, 108469. https://doi.org/10.1016/j.quascirev.2023.108469.

Żarczyński, M., Wacnik, A., Tylmann, W., 2019. Tracing lake mixing and oxygenation regime using the Fe/Mn ratio in varved sediments: 2000 year-long record of human-induced changes from Lake Żabińskie (NE Poland). Sci. Total Environ. 657, 585–596. https://doi.org/10.1016/j.scitotenv.2018.12.078.

Zhengji, Y., 2010. Microbial removal of uranyl by sulfate reducing bacteria in the presence of Fe (III)(hydr) oxides. J. Environ. Radioact. 101, 700–705.